MECHANICAL ENGINEERING DEPARTMENT

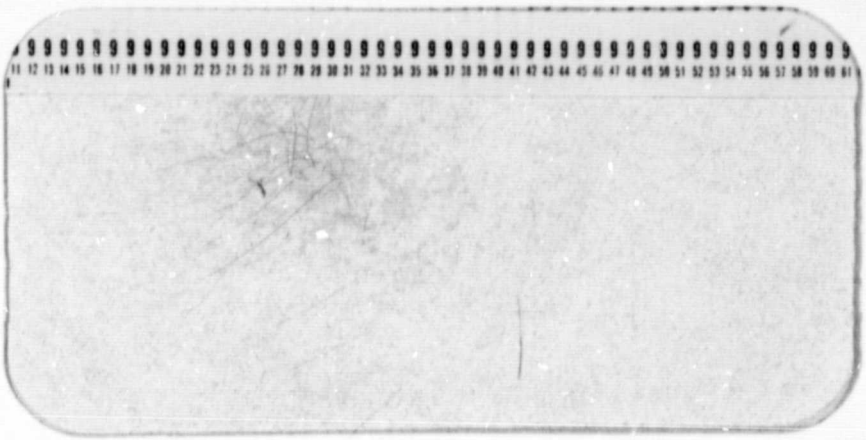

SCHOOL OF ENGINEERING
THE UNIVERSITY OF CONNECTICUT
STORRS, CONNECTICUT

TURBINE ENDWALL SINGLE CYLINDER PROGRAM

Semi-Annual Status Report

Grant No. NSG 3238

July 1, 1982 - January 1, 1983

Submitted to:

Lewis Research Center

National Aeronautics and Space Administration
21000 Brookpark Road
Cleveland, Ohio 44135

Principal Investigator:

Lee S. Langston
Associate Professor

Graduate Assistant:
Wayne A. Eckerle

Department of Mechanical Engineering
University of Connecticut
Storrs, Connecticut 06268

Introduction

The following is a report of progress made during the second six months (July 1, 1982 to January 1, 1983) under the second phase of NASA Grant No. NSG 3238. (Work is continuing to complete the final reports on the first phase of this grant).

Under this second phase, detailed measurements will be taken of the flow field in front of a large-scale single cylinder, mounted in a wind tunnel. The measurements will include static pressures on the endwall and cylinder surfaces, extensive five-hole probe pressures in front of and around the cylinder, and velocity fluctuations using a hot-wire probe where the flow is steady enough to yield meaningful results. These experiments will be conducted in the NASA two-cylinder, low-speed wind tunnel described by Langston[1-5].

These measurements will provide for a better understanding of the three-dimensional separation occuring in front of the cylinder on the endwall, and of the vortex system that is formed. They will also provide a data base with which to check analytical and numerical computer models of three-dimensional flows.

The work that will be reported on is as follows:

a) Wind tunnel test section modification.

b) Experimental model.

c) Data acquisition system.

d) Probe positioner and traverser.

e) Hot-wire instrumentation.

f) Shakedown tests.

g) Asymmetric model of saddle point flow.

Wind Tunnel Test Section Modification

The tunnel test section floor has been modified to accomodate the single cylinder and provide the required endwall static pressure taps. (The tunnel floor boundary layer will be characterized to minimize probe interference effects.) The plexiglass test section floor has been replaced by two aluminum plates whose design has been described in detail by Langston[6]. A support plate, Fig. 1, is attached to the test section frame with the remainder of the floor consisting of an instrumented disk, Fig. 2, that fits concentrically inside the support plate. The instrumented disk contains static pressure taps, mounting holes for the test cylinder, and an access hole through which the cylinder static pressure lines will be routed. In addition, indexing holes have been very accurately machined into the disk outside surface near the outer edge to indicate the disk angular location. A spring loaded pin assembly has been fabricated and attached to the support plate to serve as the reference for the disk angular orientation. A photograph of a portion of the inverted test section floor showing the indicator and indexing holes is contained in Fig. 3. Stainless steel tubing, 0.062 in. O.D. by 0.047 in. I.D., has been epoxied to each of the static taps in the support plate and the instrumented disk. All of the tubes have been pressure checked to ensure that the epoxy joints do not leak. The stainless tubes are used to connect the pressure taps with plastic tubes that mate with the laboratory scanivalve. A plug, shown in Fig. 4, has been fabricated to fit into the access hole in the instrumented disk. The plug has been installed to permit tunnel checkout testing without the cylinder installed. A photograph of the assembled test section floor, taken with the floor inverted on the work bench prior to installation into the tunnel, is shown in Fig. 5.

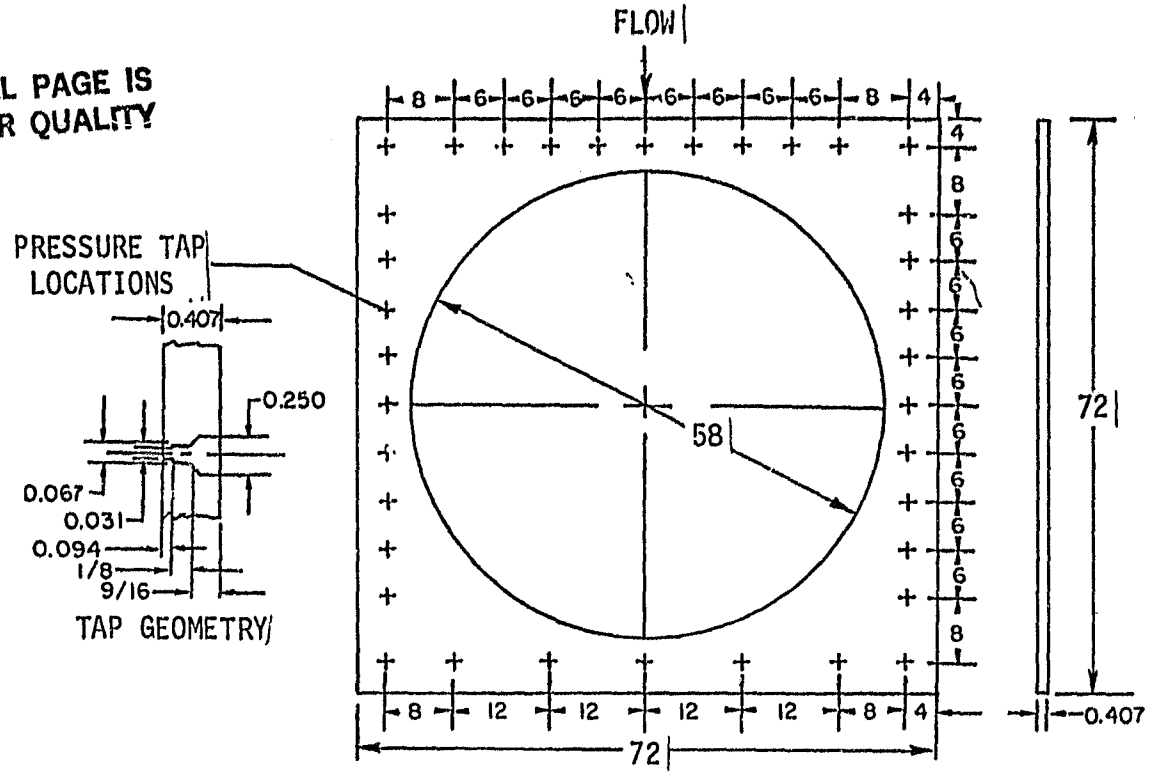

Dimensions in inches

Figure 1 Wind tunnel floor support plate

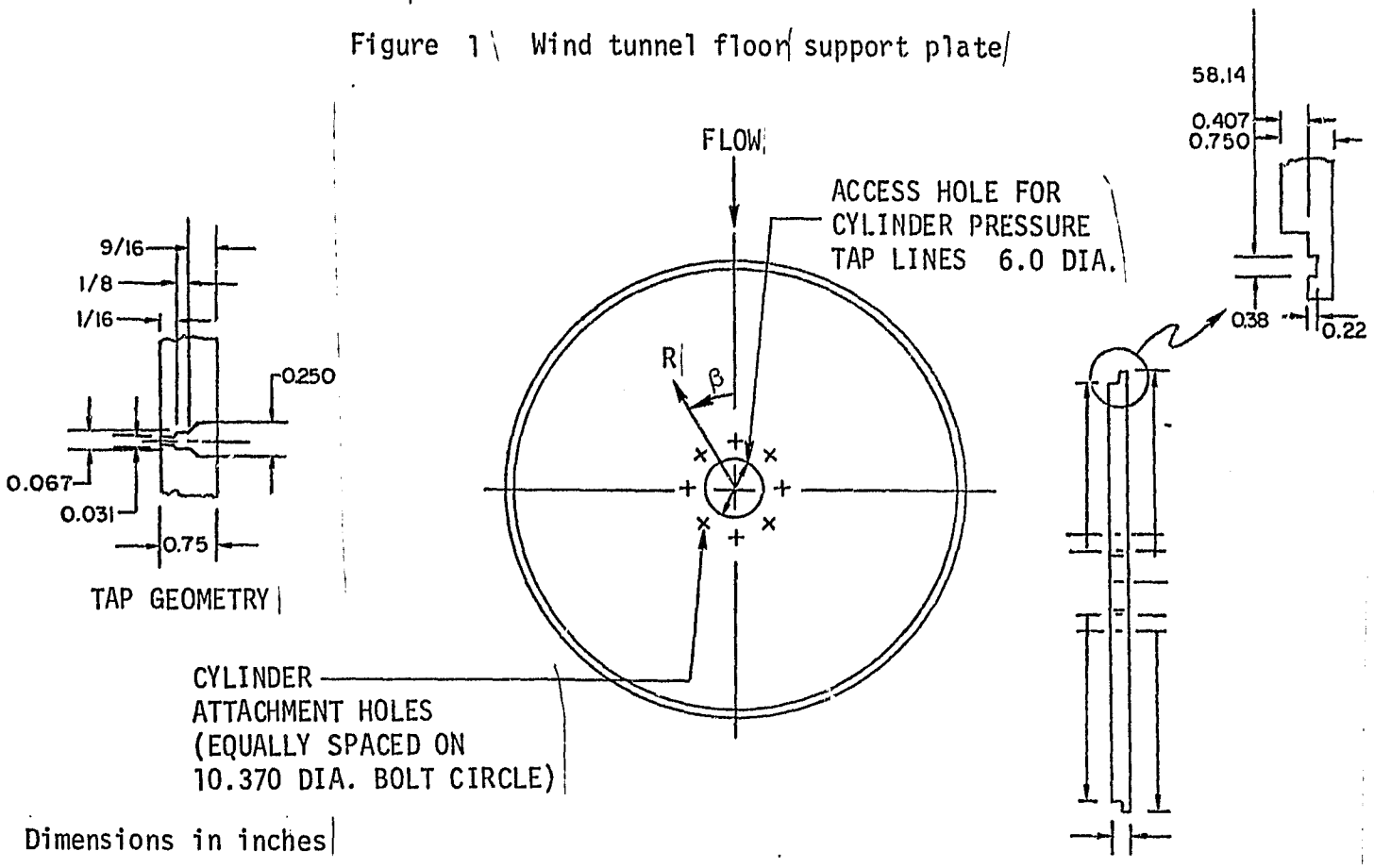

Dimensions in inches

Figure 2 Wind tunnel floor instrumented disk

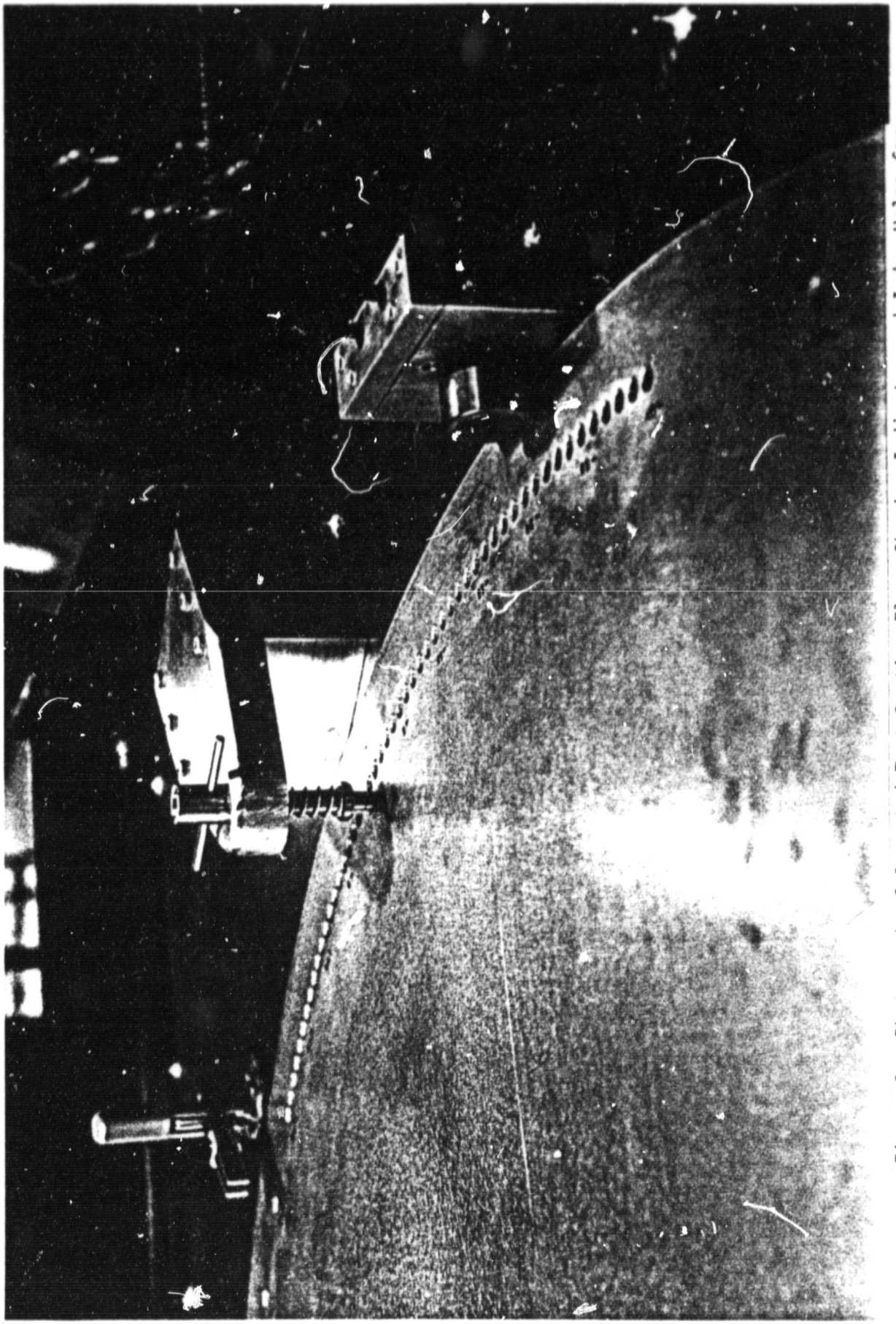

Figure 3. Photograph of Inverted Test Section Floor Showing Indicator and Index Holes for Angular Location of Instrumented Disk

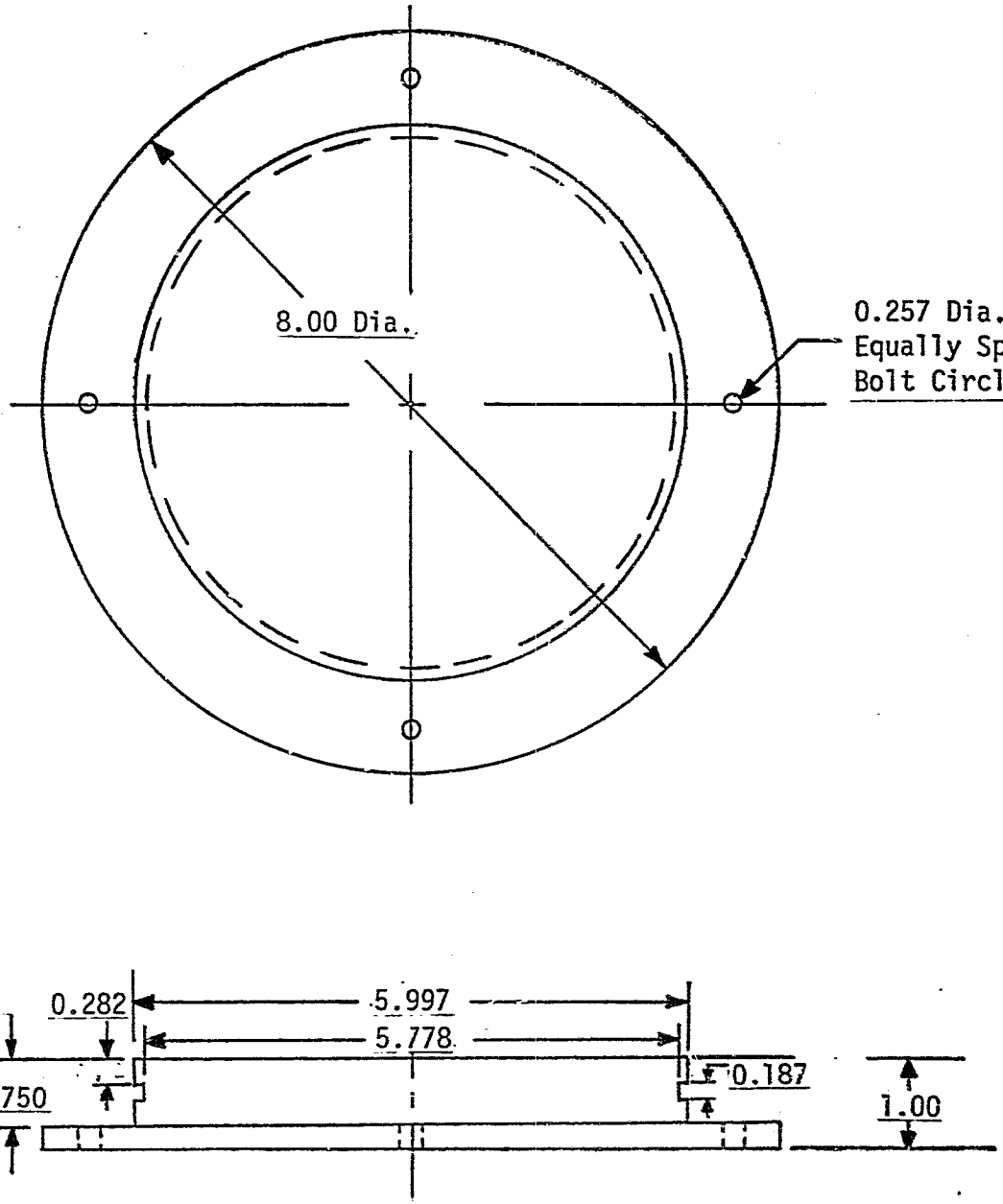

Material: Aluminum
Dimensions In Inches

Figure 4. Plug for Instrumented Disk

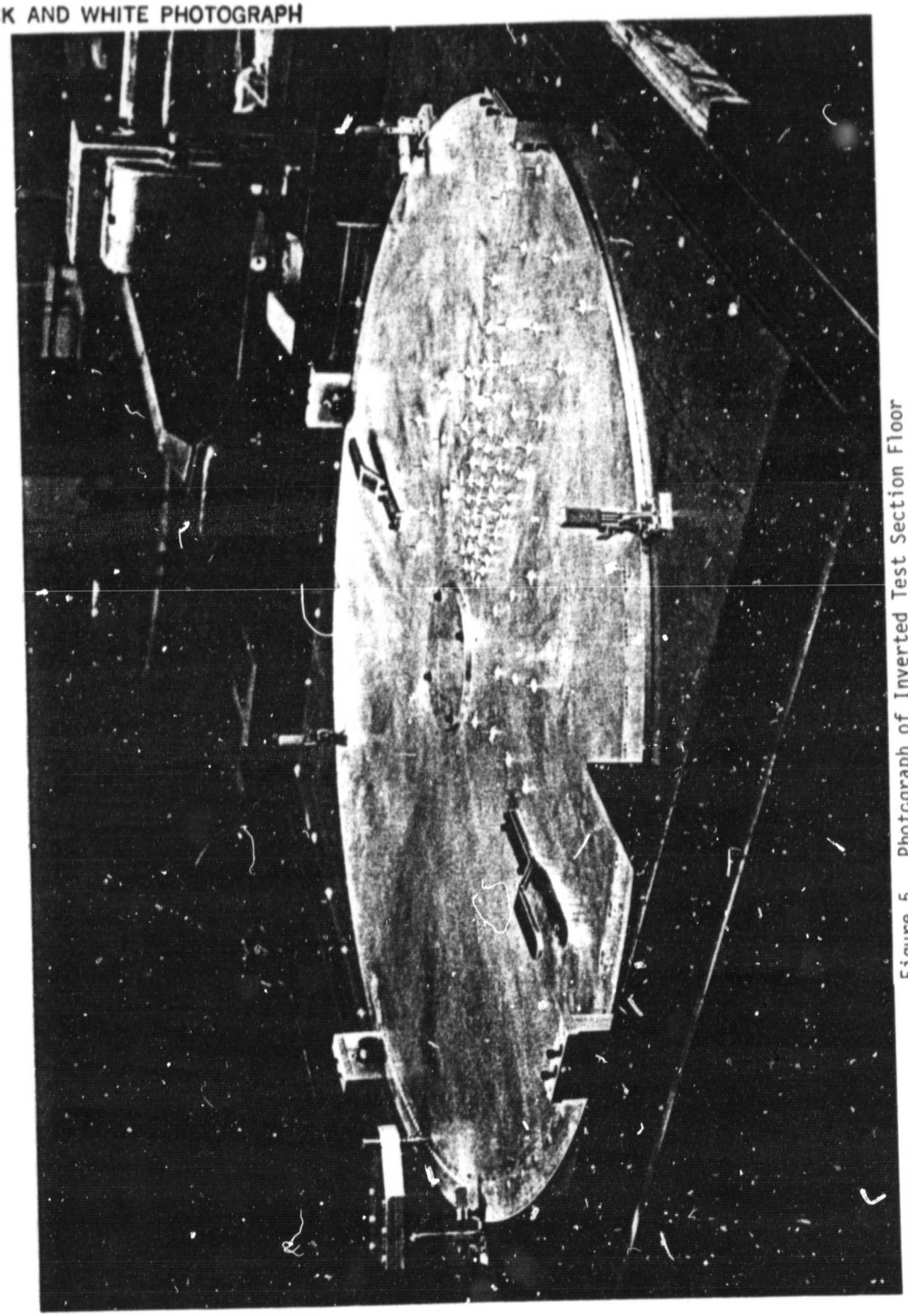

Figure 5. Photograph of Inverted Test Section Floor

With the new floor installed in the test section, the weight of the floor caused the angle iron support members to sag. Adjustable trusses were incorporated into the test section frame to minimize the sagging. By properly adjusting the trusses, the tunnel flow is flat to within 0.05 in. However, the test section height was found to vary approximately 0.2 in. The variation is mainly due to a problem with the probe positioner plates located on the test section ceiling. The probe positioner is described by Langston[5] and a photograph of the disassembled positioner is shown in Fig. 6. The plates were fabricated from rolled aluminum and were not machined flat. The plates were clamped flat when the plate edges were rabbetted. Consequently, the plates also had to be clamped when assembled in order to mate properly. This clamping was accomplished during the two-cylinder program using toggle clamps. However, the force from the toggle clamps permanently bent the perimeter plates connecting the probe positioner assembly to the test section plexiglass ceiling. Thus, the test section ceiling sags with the test section height smallest near the center of the tunnel. A solution to this problem would be to remachine all of the aluminum positioner plates out of tooling stock, but this would cause a significant delay in the test program. However, the sag in the ceiling, which is approximately 1.7 percent of the tunnel height, should only cause local flow variations and not significantly affect the core flow in the test section. Thus, the characterization of the floor boundary layer should not be affected by the sag in the test section ceiling. Measurements will be obtained during the tunnel shakedown tests to ensure that the sag in the ceiling does not affect the symmetry of the core flow.

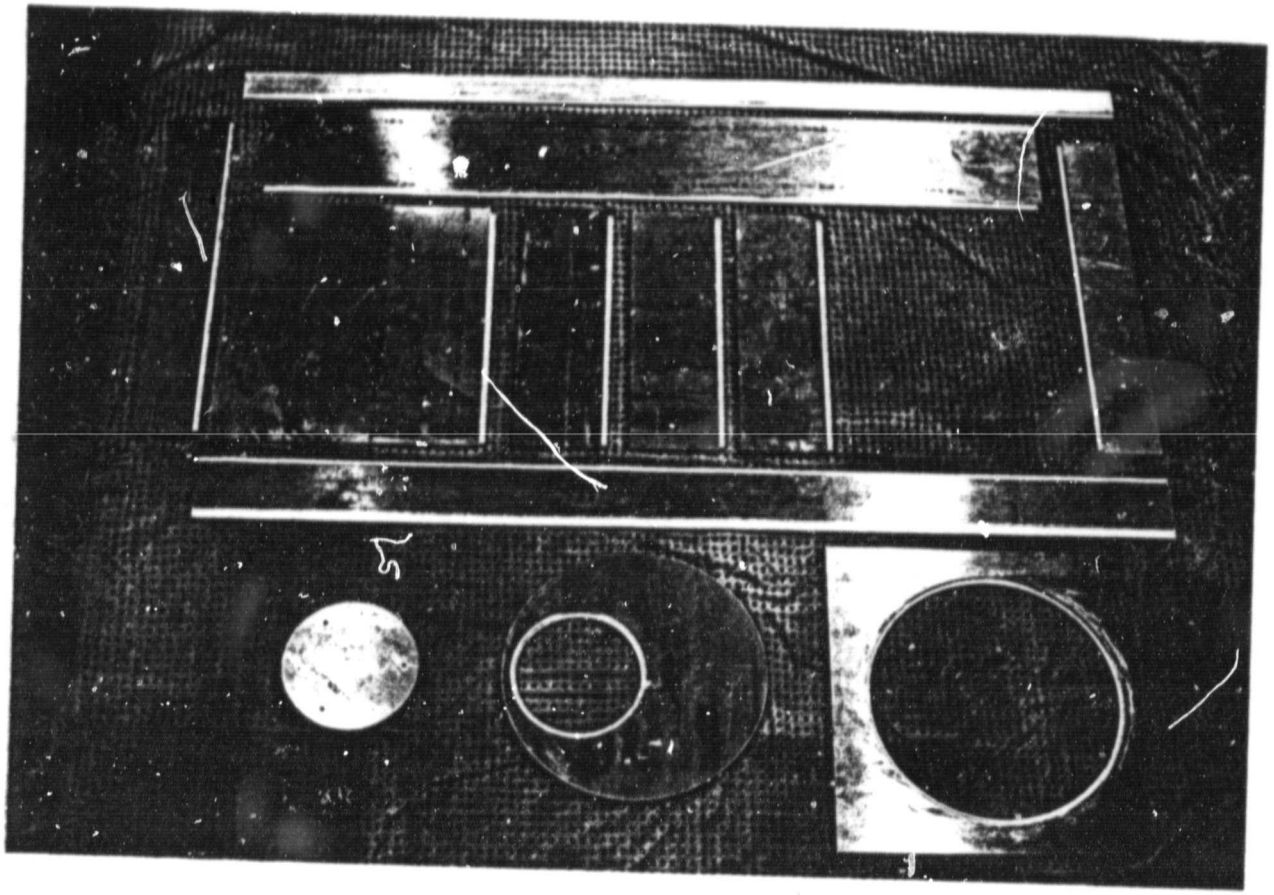

Figure 6. Probe Positioner Plates, Disassembled

Experimental Model

The experimental model is a cylinder instrumented with static taps. The design of the cylinder has been described by Langston[6] and is shown in Fig. 7. The original design called for the cylinder to be machined to a length consistent with the reassembled test section so that an O-ring could be used to seal around the cylinder. However, the sag in the test section ceiling creates a 0.041 in. variation in test section height in the vicinity of where the cylinder will be located. This variation in height is too large to be mitigated by O-ring compression. As an alternative, a cylinder height was chosen so that a 1/8 in. foam rubber type gasket can be used for the compression seal around the top of the cylinder. This type of gasket can withstand the required compression without imposing large loads on the stationary disks of the probe positioner. A sketch of the final cylinder design is shown in Fig. 8. A lip has been machined into the cylinder top surface to hold the gasket and counteract the shear forces imposed on the gasket by the rotating positioner disks. In addition, a disk with an O-ring seal was installed inside the cylinder to stop ambient air from leaking through the inside of the cylinder into the test section (see Fig. 8). Thus, the gasket material must only seal against the pressure gradient around the outside of the cylinder.

Stainless steel lines were epoxied in the pressure tap holes and leak checked. The tubes were routed out of the center of the cylinder base inside a six inch diameter circle corresponding with the access hole in the instrumented disk. As with the test section floor, the stainless steel tubes will be connected to the laboratory scanivalve via plastic tubing.

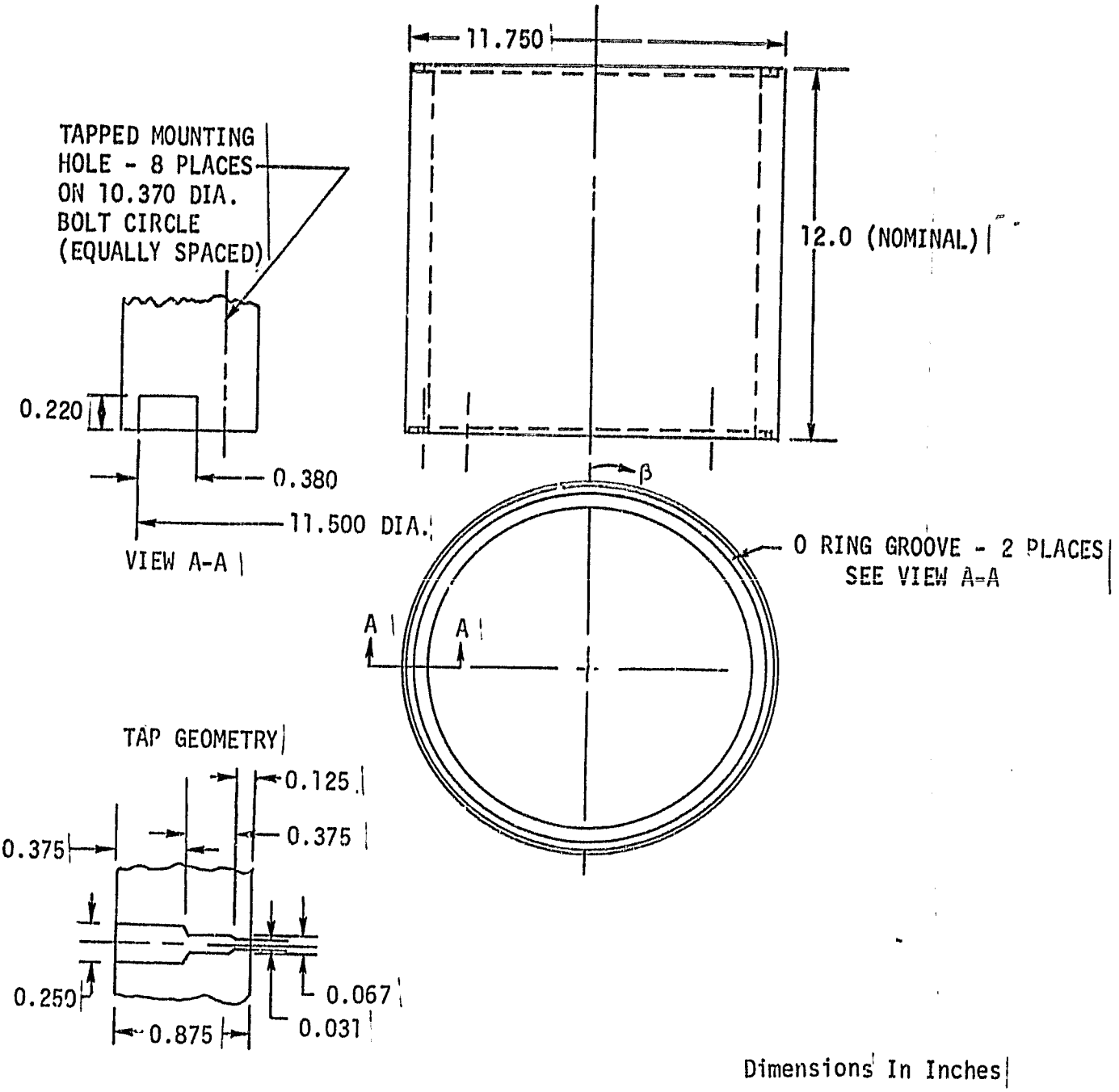

Dimensions In Inches

Figure 7. Cylinder test model

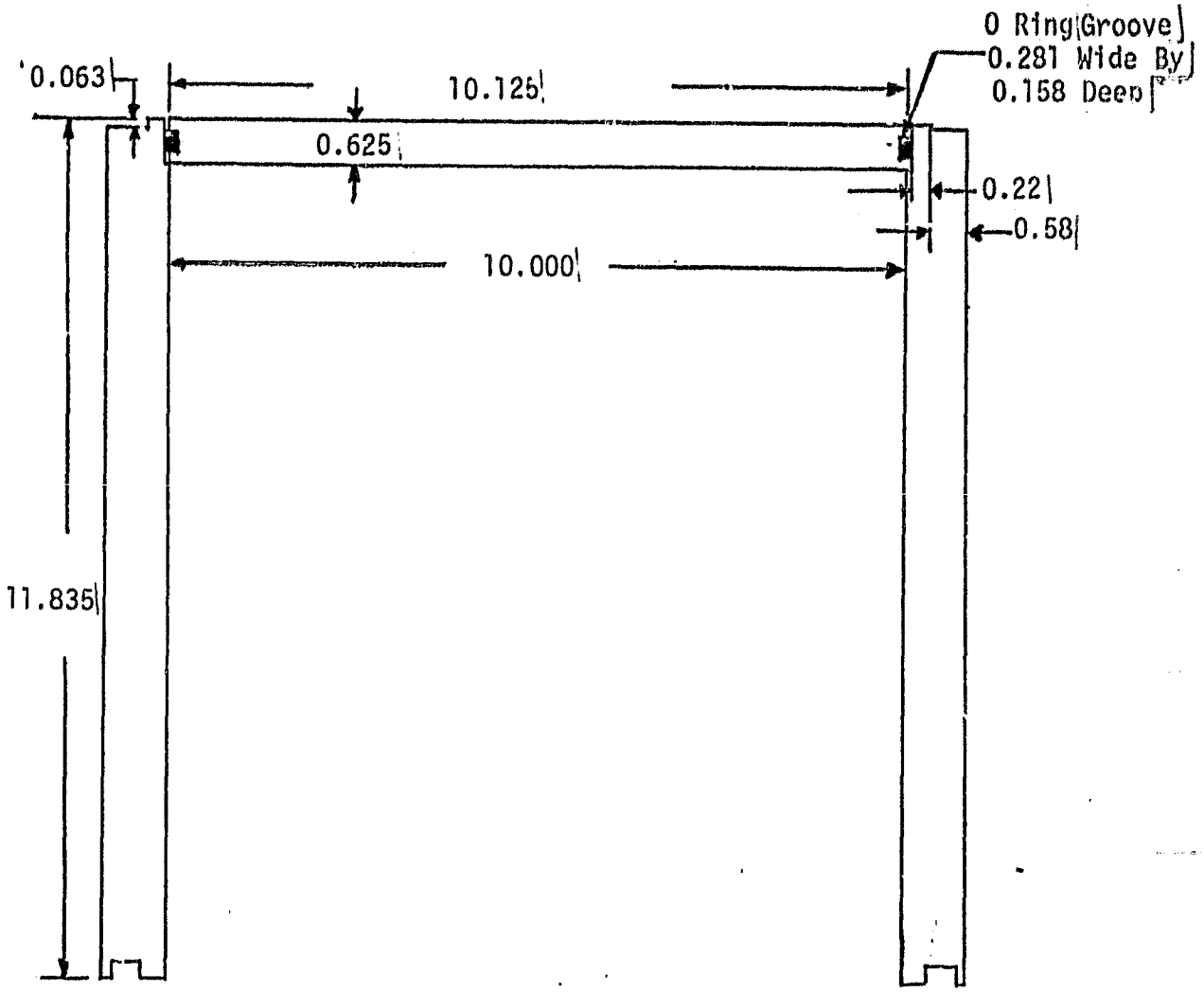

Figure 8. Cross-sectional View of Final Cylinder Design

During the initial phase of the test program, an afterbody will be installed downstream of the cylinder. The purpose of the afterbody is to displace the separation downstream of the cylinder and thereby eliminate the unsteadiness introduced into the flow by the cylinder wake shedding. Provided that the presence of the afterbody does not alter the upstream separation, the reduction in unsteadiness should allow flow data to be acquired further downstream from the leading edge of the cylinder. A sketch of the afterbody design is shown in Fig. 9. The afterbody is fabricated from aluminum and consists of two side plates connected by three braces for rigidity. The upstream edge of the afterbody has a machined radius that will mate to the cylinder. Gasket material will be installed on all edges to stop any leakage around the afterbody. The difference in the upstream and downstream afterbody height is required due to the sag in tunnel ceiling discussed above. Fabrication of the afterbody has been completed. When installed, the afterbody will be bolted to the test section ceiling.

Data Acquisition System

The main component to be used for acquiring steady state experimental data for this test program is an ADAC Corporation data acquisition system (DAS). The system, described by Langston[6], has been updated with the installation of a 1664 TTL input/output board. This board enables the data system to send and receive signals across 64 ports. In particular, with this board the DAS can be used to control the scanivalve stepping. A control circuit has been designed and built to interface between the 1664 TTL board and the scanivalve. The DAS can now be utilized to step the scanivalve as well as receive a signal indicating the current scanivalve position.

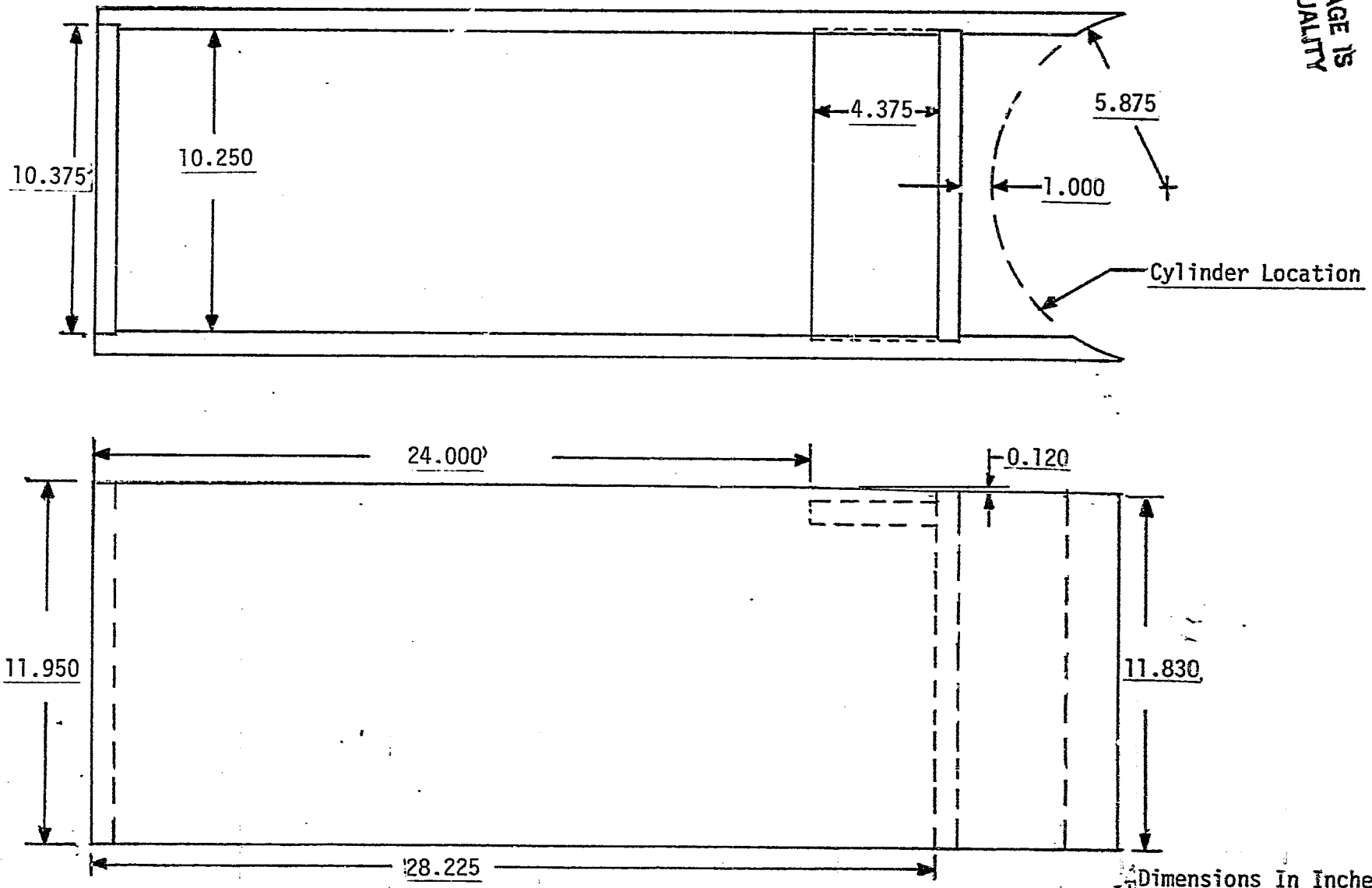

Figure 9. Afterbody for Test Cylinder

A layout of the various components to be used with the DAS is shown in Fig. 10. The overall instrumentation setup involves connecting the various static taps and probes to the laboratory scanivalve box. The box contains a model SSS-48 CBM 48-port scanivalve that can sequentially connect each pressure to a single Barocell differential pressure transducer (Gould type 590). The output from the transducer is integrated and sent to a Hewlett Packard (HP) model 3455A digital voltmeter. The voltmeter is accessed by the DAS through an IEEE buss. The transducer signal is not sent to the DAS analog to digital (A/D) converter because the converter resolution of 0.0012 volts is not low enough to accurately convert the millivolt signal from the transducer. The HP voltmeter A/D converter, with a resolution down to the microvolt range, can accurately resolve the transducer signal. Other experimental outputs, such as flow temperature and probe position, will be converted using the DAS A/D converter. All data will be recorded on an 8 inch floppy disk from which the data can be accessed for reduction. The reduced data can be printed on an Axiom IMP miniprinter so that the experimental data can be analyzed immediately after it is acquired.

The Barocel transducer has been calibrated using a Von Essen-Delft type 250 Betz micromanometer accurate to 0.0004 in. H_2O. The transducer calibration is very nearly linear (a least squares linear curve fit has a standard deviation of 0.00043) so that the laboratory pressure reference system will not be needed to check the calibration during tests. Instead, one pressure and the transducer reference pressure will be connected to the Betz micromanometer. The manometer reading will be hand recorded for each run and compared with the value calculated from the transducer reading. This comparison will indicate the

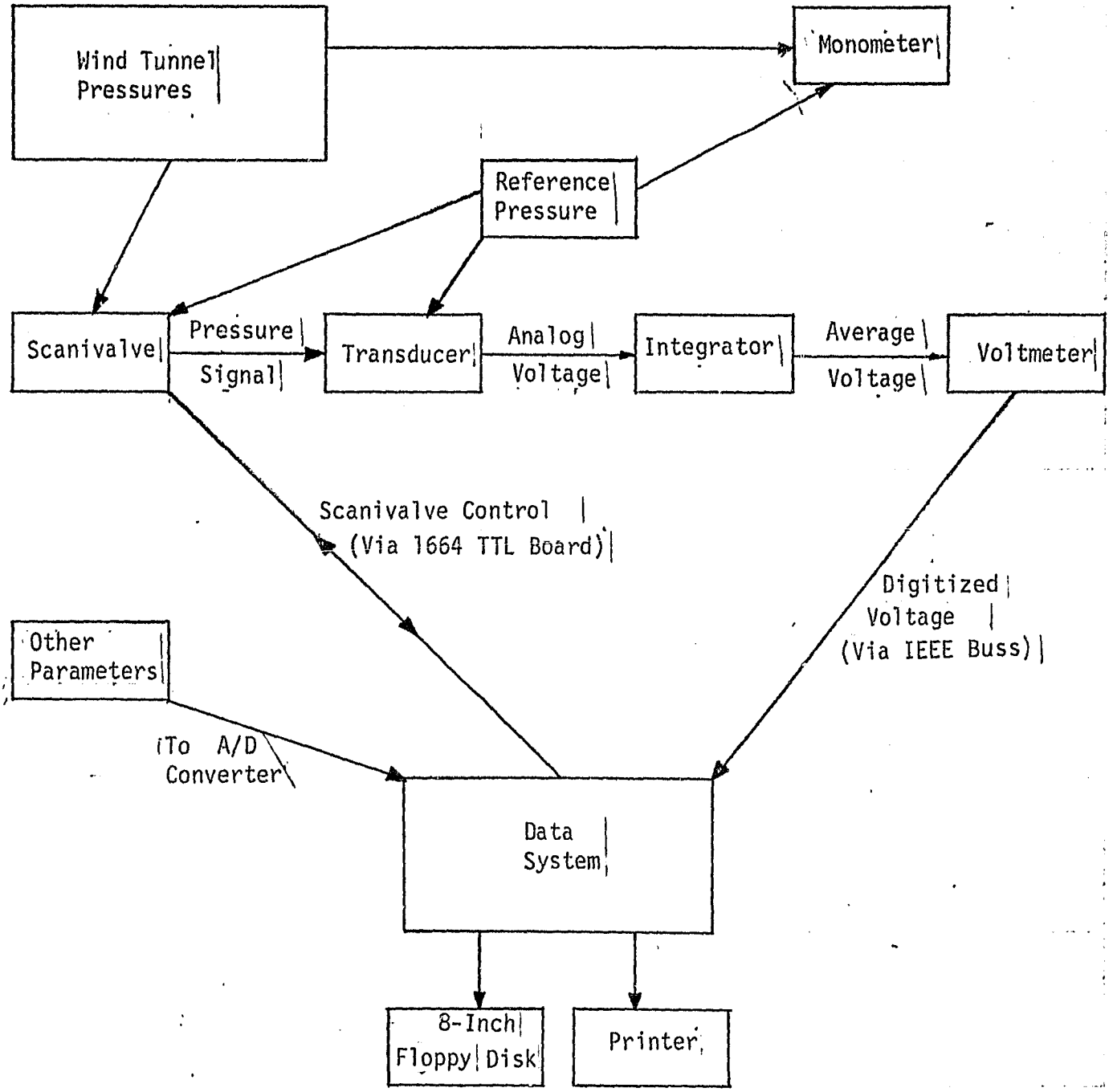

Figure 10. Data Acquisition Instrumentation

accuracy of the calibration as well as a continual verification that the calibration has not changed. In addition the transducer reference pressure will be connected to one scanivalve port so that the transducer zero is recorded for each test run.

A program has been developed for acquiring data using the DAS. A flow chart of that program is contained in Fig. 11. Initially the program reads constants that control the acquisition process from a scratch file. The constants include the run number, the number of channels and number of samples to be collected from the DAS A/D converter, the number of ports on the scanivalve to be sampled as well as the number of samples to be gathered from each port, the scanivalve stepping rate, and the barometric pressure at the beginning of the run. By allowing the values of these constants to be changed external to the program, the program has the flexibility to be used for a variety of instrumentation set-ups. The program opens a data file and assigns the current run number to that file. The acquisition constants along with the current time and date are entered into the file for reference purposes. Data from the DAS A/D convertor are then collected, and the converted voltages are stored in the data file. The collection rate is manually set on the DAS A/D board, which can sample up to 12kHz. The program then records the signals from the scanivalve transducer in the following manner. The program sends the scanivalve to its home port and reads the output signal from the scanivalve to ensure the scanivalve has stepped properly. The program waits a specified period (15-20 seconds) for the signal to be integrated. The transducer signal is then recorded from the HP A/D converter using the IEEE buss instrumentation. The transducer signal is recorded at a slow rate (2 Hz) for 10-25 seconds (20-50 samples) to resolve low

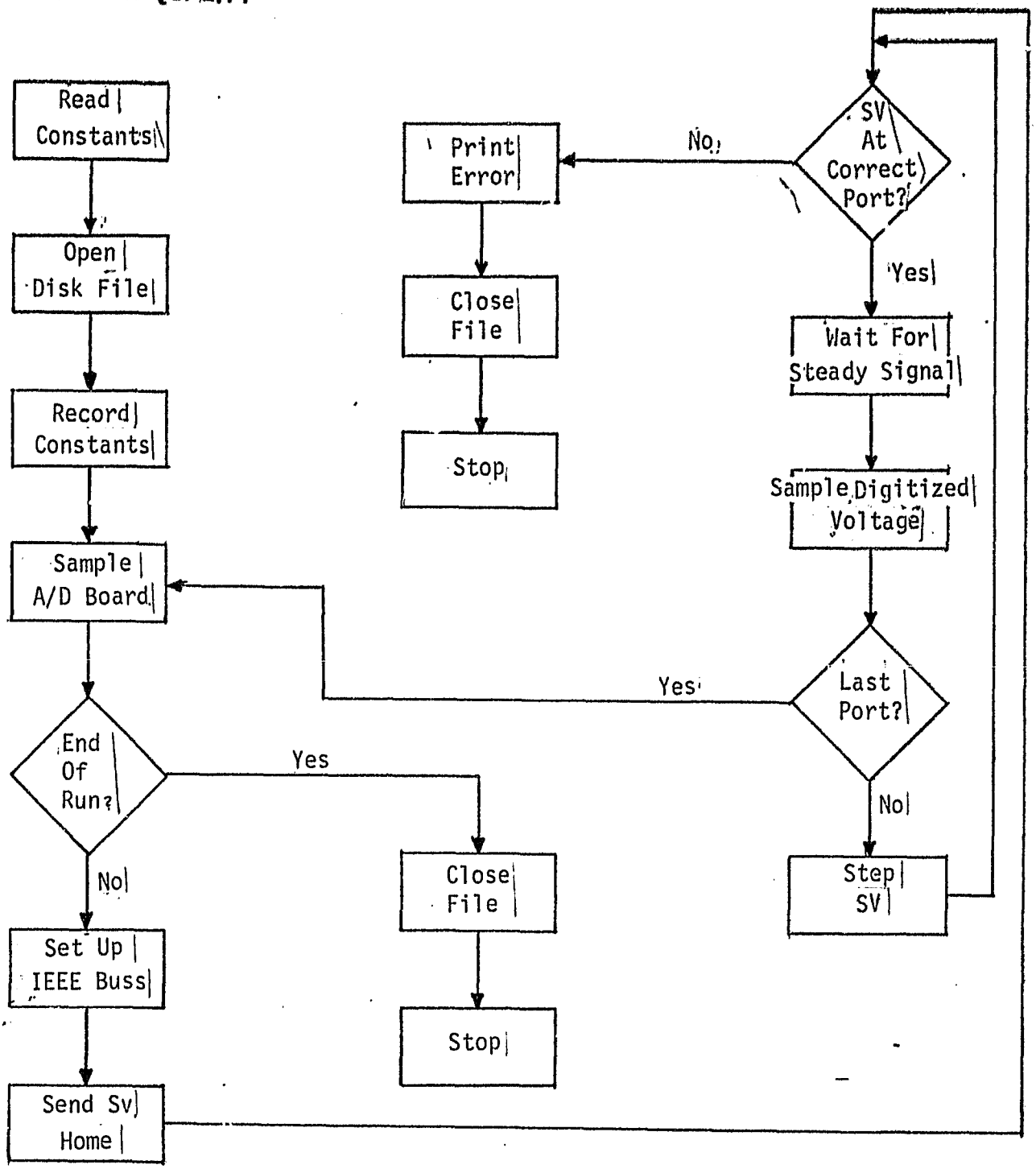

Figure 11. Data Acquisition Program Flow Chart

frequency oscillations in the integrated signal. The program then successively steps the scanivalve repeating the above process for the number of ports defined by the acquisition constants. The program finally collects data from the DAS A/D convertor a second time at the end of the run and closes the data file. Thus, the outputs connected to the DAS A/D board can be averaged over the duration of the run.

A reduction program has been written to reduce the acquired data. The program reads the data from the data file on the floppy disk, averages the samples, computes average and standard deviations, and converts the pressure data to pressure coefficients using the formula:

$$C_p = \frac{P-P_{ref}}{(P_T-P)_{ref}}$$

where $P-P_{ref}$ is the pressure calculated from the transducer signal using the transducer calibration and $(P_T-P)_{ref}$ is the difference between the core flow total and static pressures measured by a pilot-static probe near the south side of the test section entrance. In addition, the program calculates the average test section entrance velocity and velocity head for the run based on the reference pressures.

While the reduction program provides the opportunity to analyze the data immediately after acquisition, another program has been acquired that enables the DAS to transfer the data to the university computer center's IBM 2081 computer through a telephone hook-up. The DAS acts as a remote terminal and can be used to assemble, reduce, and plot the data using the IBM computer. One problem with this transferring technique is that the transfer rate is limited to a baud rate of 300. This limit is imposed by the modem used for the telephone hook-up and

software restraints. Efforts are under way to modify the software so that the data can be transferred to the IBM computer across the 9600 baud line from the Mechanical Engineering computer laboratory.

Probe Positioner and Traverser

The five-hole and hot-wire probes will be accurately positioned in the test section with a combination positioner and traverser. The traverser holds the probe, provides up and down motion, and rotates the probe while the positioner provides transverse and upstream/downstream motion. Two mechanical engineering seniors have previously designed and built the positioner (Fig. 6). The positioner assembly includes two stationary disks shown in Fig. 12, a small disk of 4-3/16 in. diameter inside a larger disk of 9-3/8 in. diameter. The disks have been motorized by another senior as shown in Fig. 13. Gears are installed on top of the positioner plates with a spacer plate used to raise the smaller gear above the larger gear. D.C. motors and potentiometers have been connected to the gears so that the gears can be remotely positioned and their angular location accurately determined from the potentiometer outputs. The probe tranverser, an L.C. Smith model BBR 16360, is mounted to the small gear so that a probe can extend through a hole in the gear and positioner plates to the test section. A probe can be moved anywhere in a 15.75 in. diameter circle, without shutting down the tunnel, by turning the small and large disks. Additional movement either across the tunnel or in the streamwise direction can be accomplished by shutting down the tunnel and interchanging the support plates shown in Fig. 6.

Several improvements to the positioner assembly have been made during this reporting period. The potentiometer connected to the small gear was not fitted with a backlash gear, as was done for the large gear, during the initial assembly

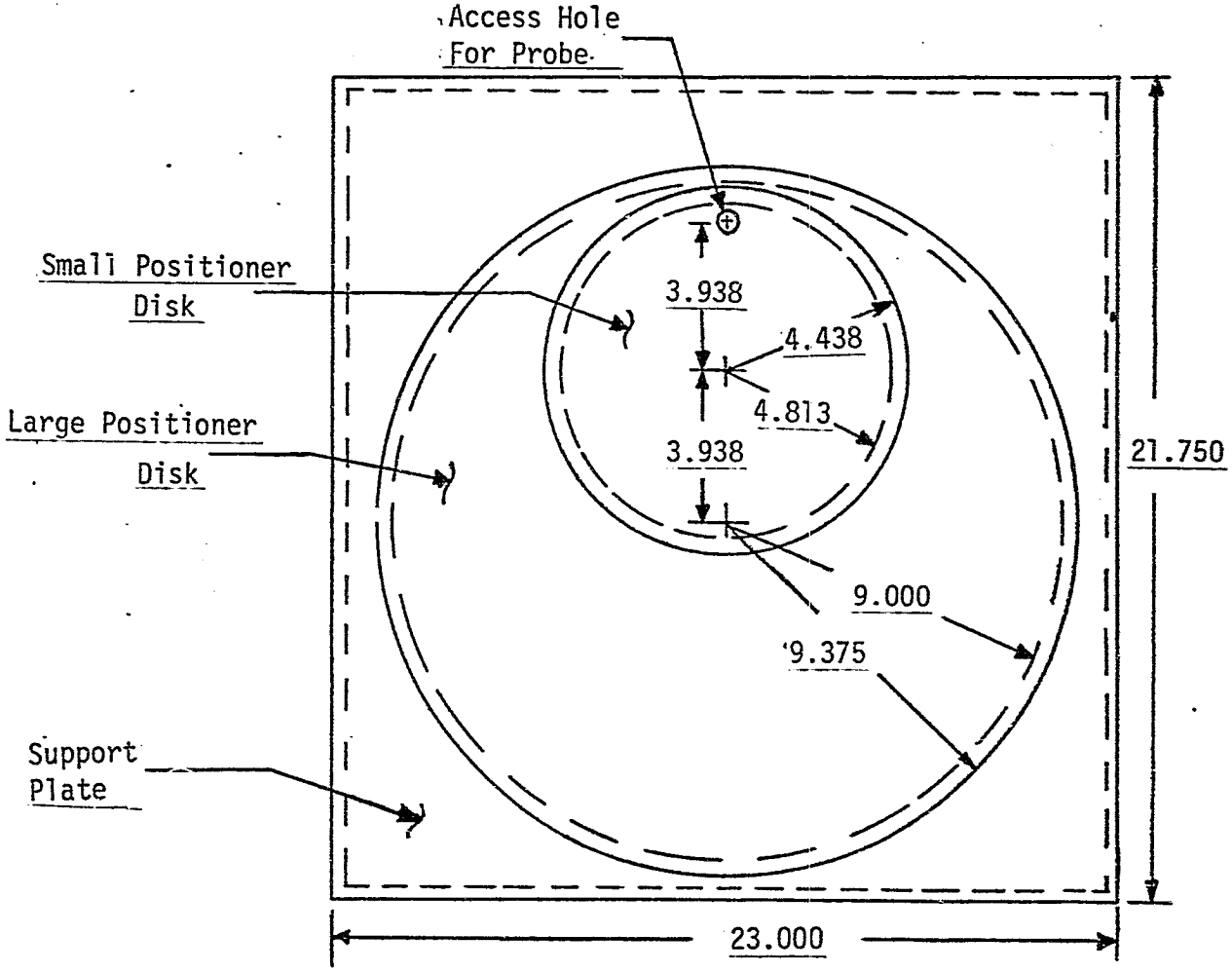

Dimensins In Inches.

Figure 12. Probe Positioner Disks

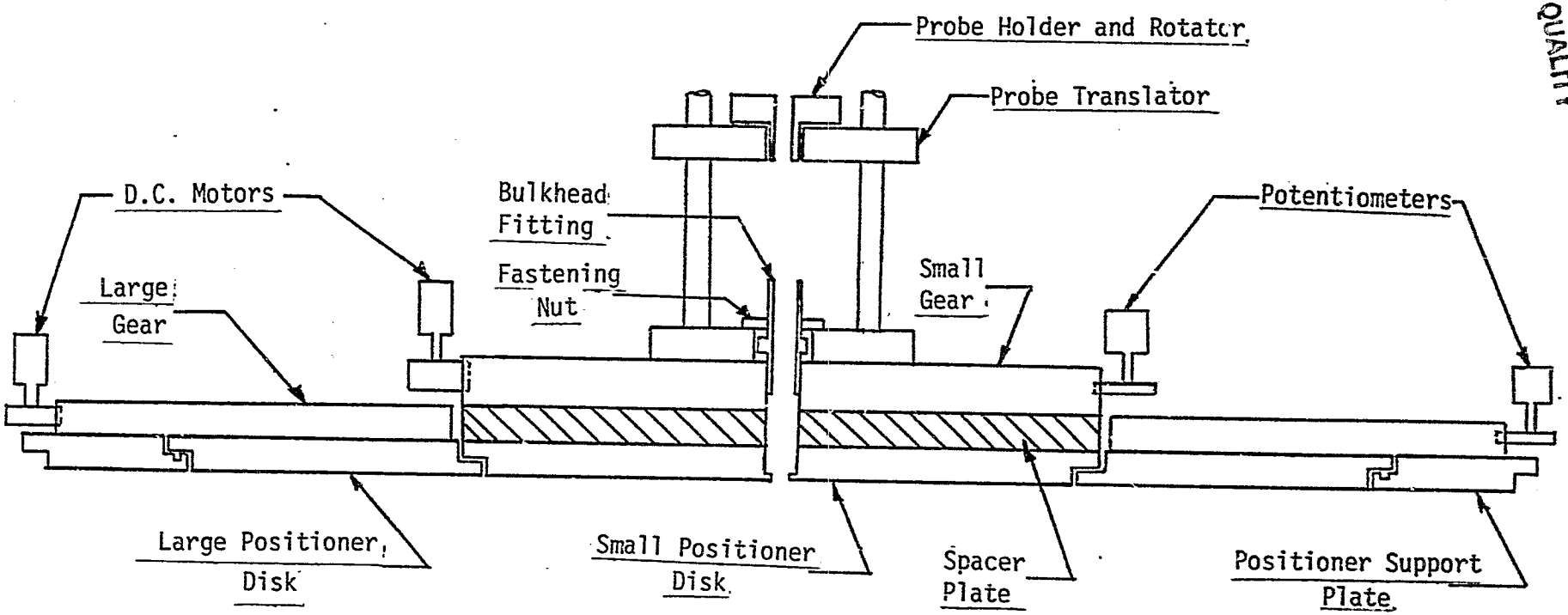

Figure 13. Cross-sectional View of Motorized Probe Positioner with Mounted Probe Traverse

because a commercially available gear that would mate with the small positioner gear was not available. However, a backlash gear has been designed and fabricated to mate with the small gear and the potentiometer in order to eliminate hysteresis in this potentiometer output. The gear has been installed in the positioner assembly.

A second improvement to the probe positioner involved installing a teflon gasket between the large and small positioning disks. In the initial configuration, the small disk's rabbetted edge rotated directly on top of a mating edge in the large disk. Since both disks are fabricated from aluminum, rotation of the small disk caused the two surfaces to chafe. During the two cylinder program, vacuum grease was used as a lubricant to reduce the chafing and provide a seal. However, the grease would be sucked into the test section allowing the disks to start chafing and eventually seize together. To avoid this problem a 1/16 in. thick teflon gasket was installed between the plates. The rabbeted edge of the small positioning disk was remachined so that the gasket could be installed without recessing the disk from the test section ceiling.

Another problem with the probe positioner involved installing and removing a five-hole probe. The five-hole probe stem has a shephard's crook as shown in Fig. 14. Therefore, the access hole in the probe positioner assembly had to be greater than 0.5 in. to allow passage of the probe into the test section. The bulkhead fitting used to mount the traverser to the small disk also had to be bored out and could not be used to seal around a probe. Instead, a seal to prevent leakage of ambient air from passing around the probe shaft into the test section was located in the smaller positioning disk. A detailed sketch of this disk is shown in Fig. 15. The disk contained a 3/8 in. diameter hole and a small passage to reduce the disk thickness near the hole. This configuration allowed the

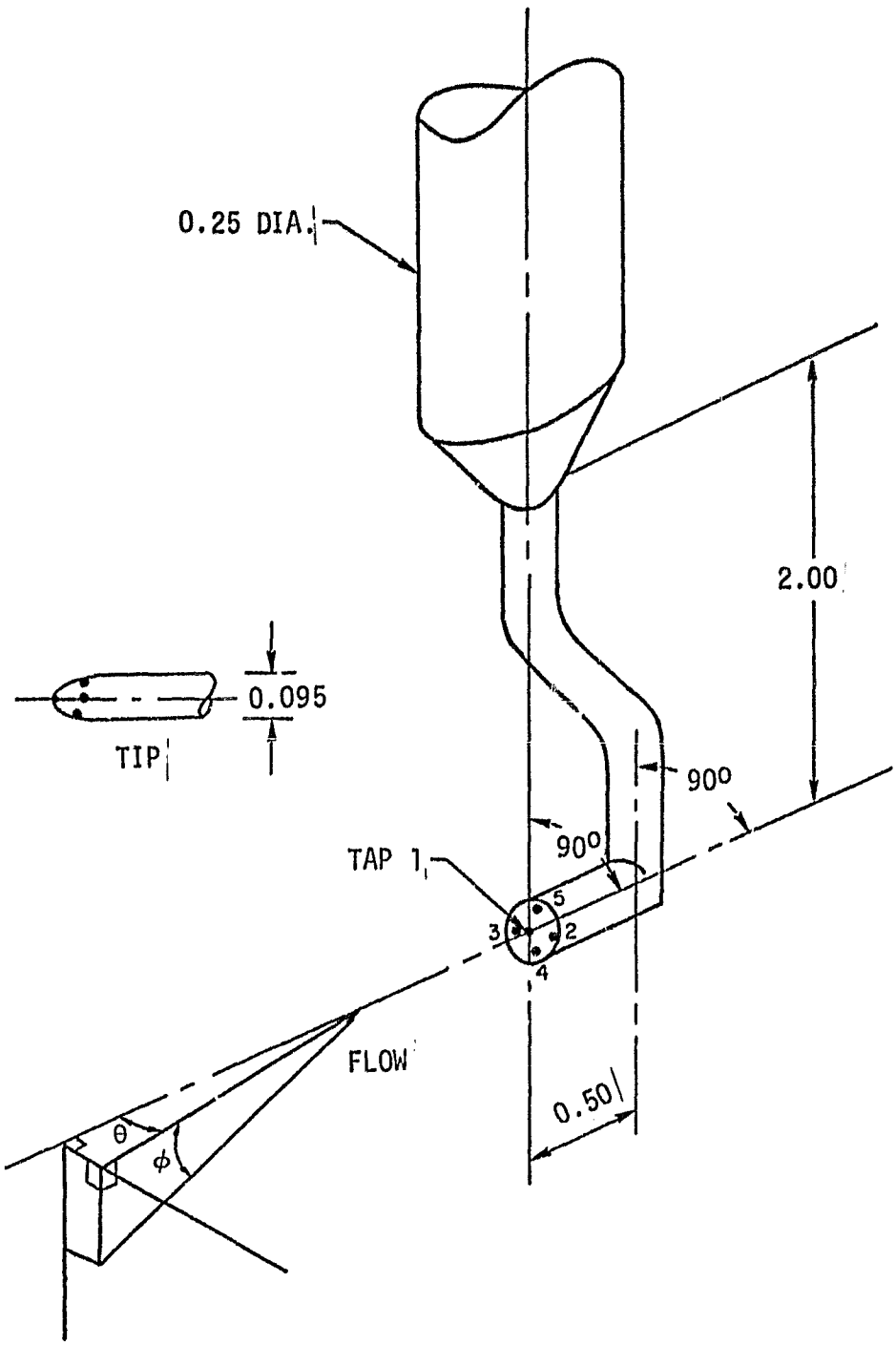

Figure 14. Five-hole probe configuration

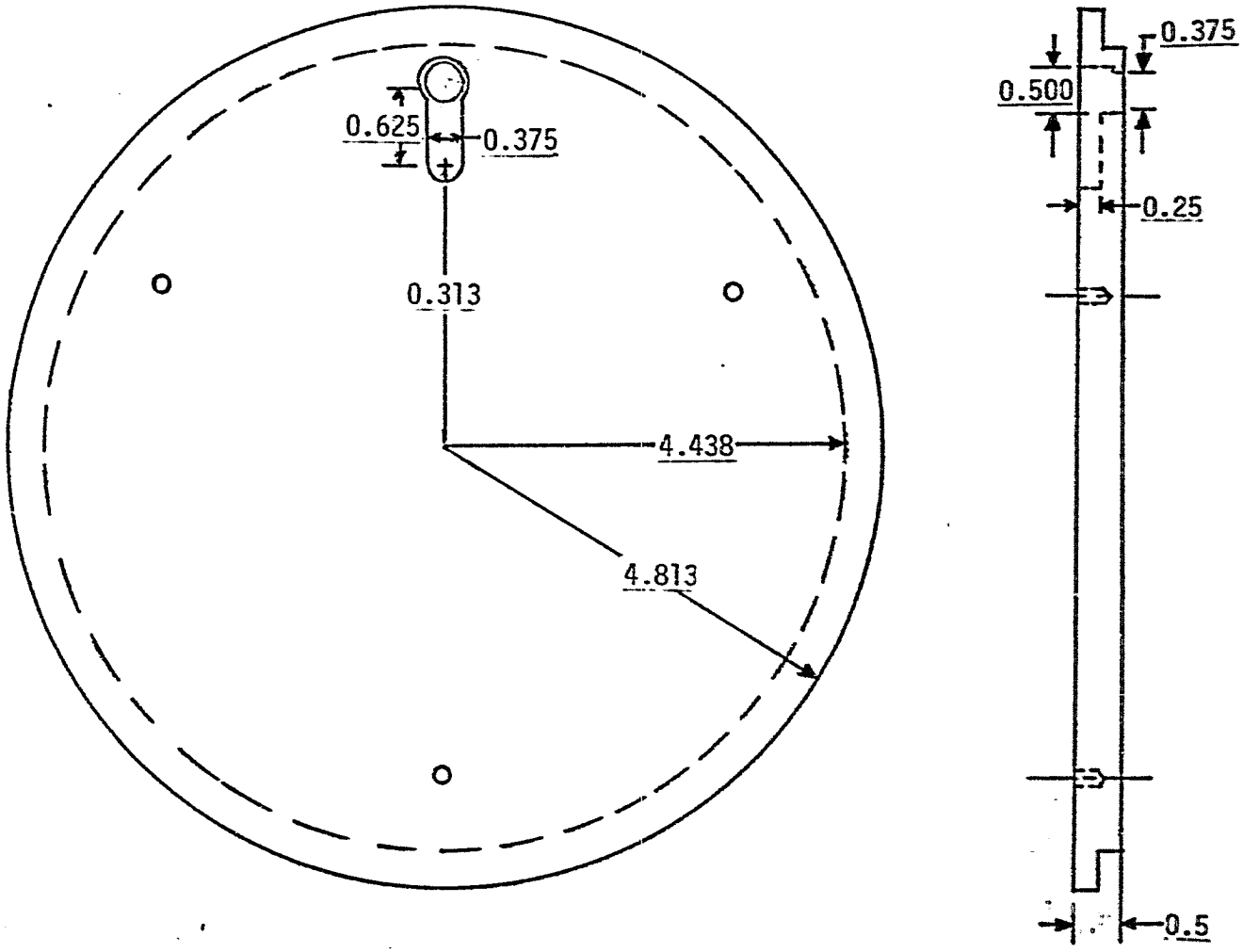

Dimensions In Inches

Figure 15. Original Small Positioner Disk

disk to be slipped over the probe tip. A seal around the probe stem was accomplished by compressing a rubber washer sandwiched between two steel washers seated in the small disk with a long sleeve extending up to the bulkhead fitting as shown in Fig. 16. The problem with this configuration was that the positioning plate was fastened to the spacer plate with screws threaded into the top of the positioning disk. Thus, the screws could not be reached unless the probe traverser and small gear were removed from the probe positioner assembly. Removal and installation of a probe, then, was very unwieldly due to the weight and size of the traverser and small gear. Extreme care had to be taken to avoid bending a delicate probe during the removal and installation process. To avoid this problem, the small positioner disk was modified. The portion of that disk involved with sealing around a probe was bored out as shown in Fig. 17 and replaced with a removable plug shown in Fig. 18. The removable plug has the same geometry as the section it replaces but fastens to the bottom of the spacer plate so that the plug, along with the sealing components, can be slipped over the installed probe from inside the test section. Thus, with the plug removed, a five-hole probe can be installed or removed with the probe traverser and positioner assembly intact on the test section ceiling.

The probe traverser has also been retrofitted. The traverser specifications include the capacity to rotate a probe about its axis over a 360 deg. range. However, the rotation was limited to an effective range of approximately 350 deg. due to limits in the potentiometer. Since this limit was a minor problem during the two-cylinder program, the traverser has been retrofitted with new gearing as that the effective range of rotation is now approximately 370 deg.

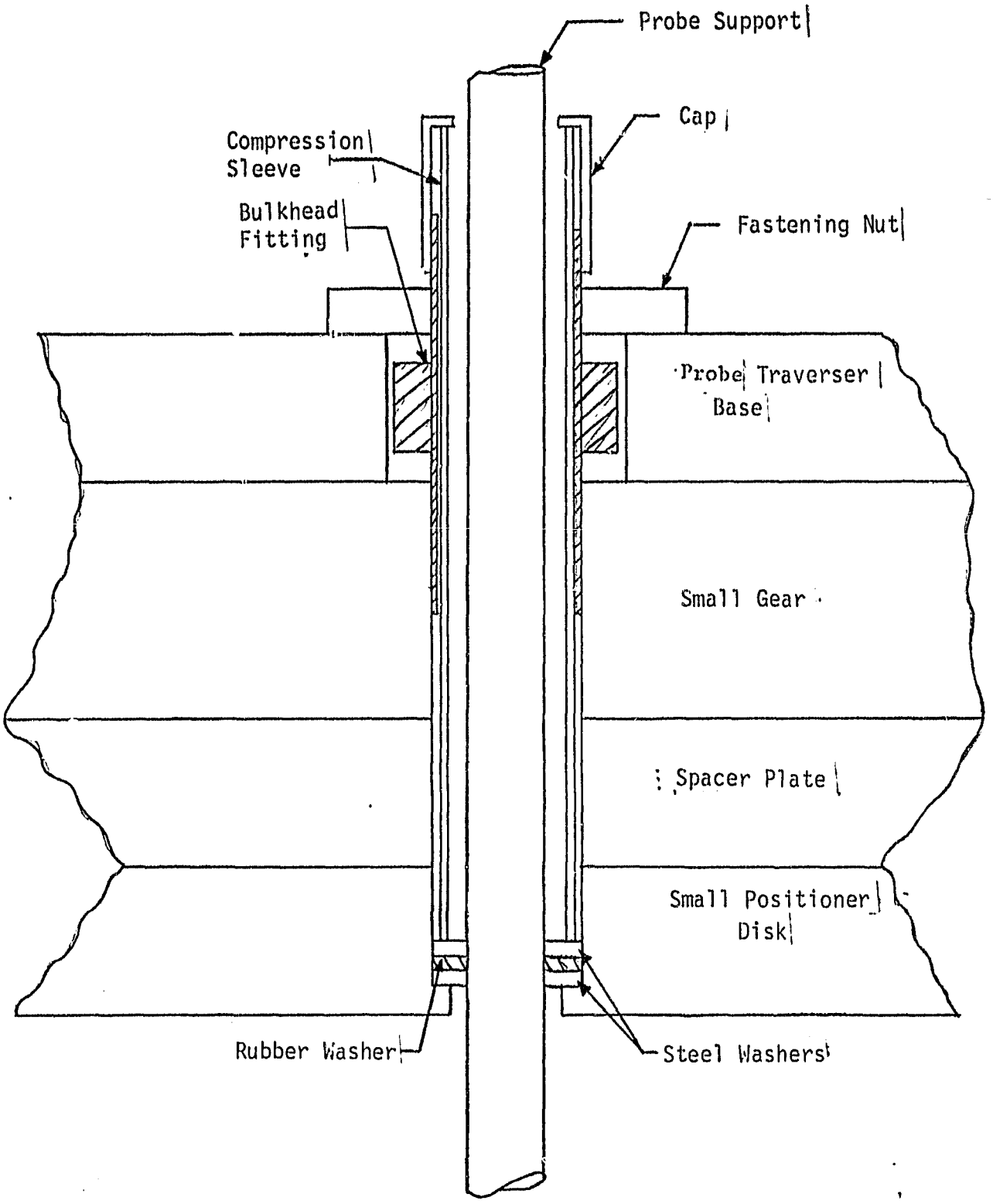

Figure 16. Seal Around Probe Support in Probe Positioner

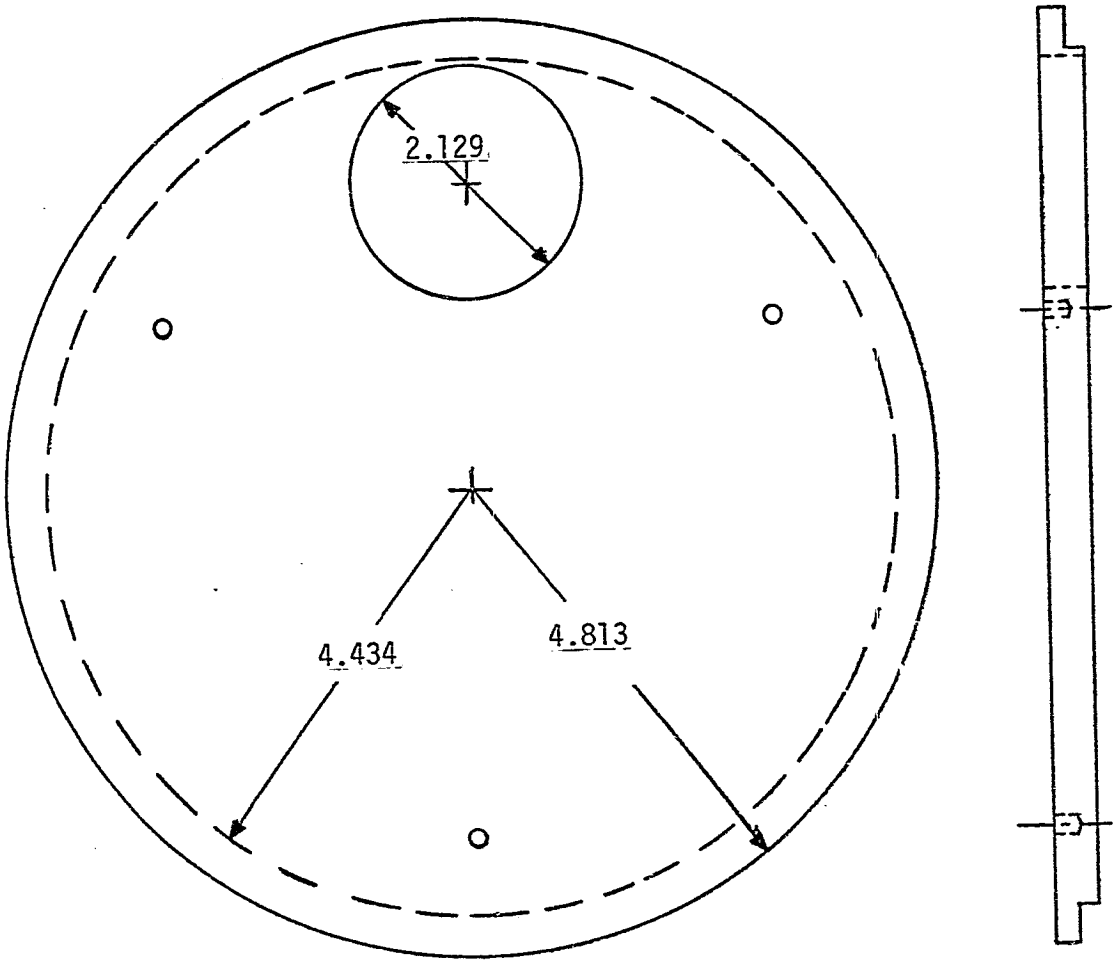

Dimensions In Inches

Figure 17. Modified Small Positioner Plate.

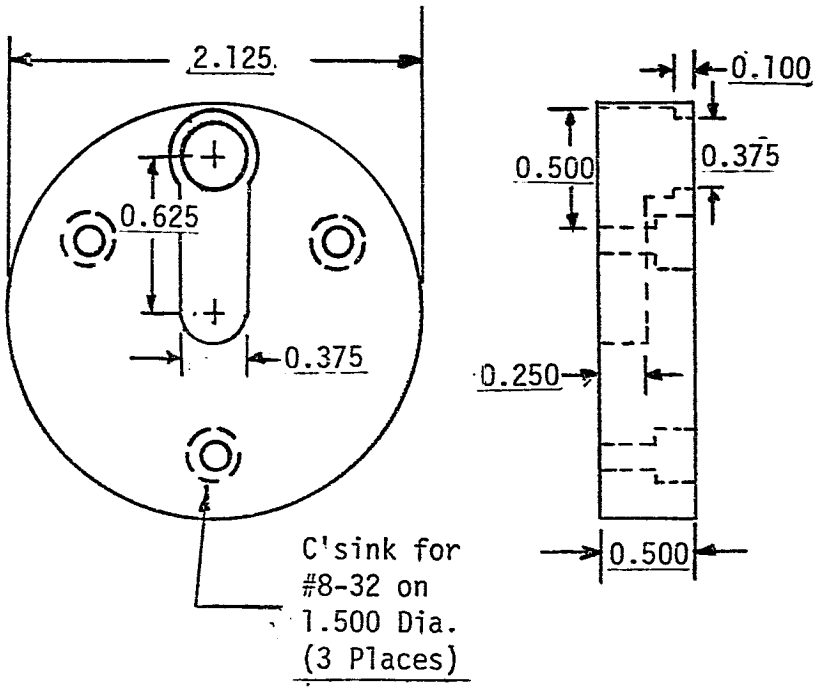

Dimensions In Inches
Material: Aluminum

Figure 18. Removable Plug for Small Positioner Disk

The modified probe positioner and traverser have been installed on the test section ceiling and checked out. The two probe positioner potentiometers and the two traverser potentiometers have been calibrated. The accuracy of the probe positioner calibrations were checked by using the calibrations to locate a probe at prescribed points on the test section floor. A grid was placed on the floor to accurately locate the probe position. The test results indicate that the positioner can locate a probe within a 0.015 in. diameter circle about a desired location. Similar checks of the traverser indicate a probe can be positioned vertically within 0.020 in. and angularly within 0.2 deg.

Hot-Wire Instrumentation

During this test program velocity fluctuation will be obtained using a hot-wire probe. The equipment that is available for these measurements is a TSI Model 1050 series anemometer. The system includes a Model 1050 constant temperature anemometer, Model 1051 monitor and power supply, Model 1052 digitizer, and a Model 1057 signal conditioner. A probe support compatible with the L.C. Smith probe traverser has been procurred along with a TSI Model 1012 straight hot-film probe. A hot-film as opposed to a hot-wire probe will be used for these measurements because of the hot-film probe's higher durability. The fine wire in a hot-wire probe could not withstand the small particles that are ingested into the tunnel from the room. The hot-wire system is presently being assembled in the laboratory and will be checked out during the tunnel shakedown tests. Additional hot-film probes, such as a cross- or slant-film probe, will be purchased as required to resolve the velocity fluctuation components. However, a survey of the flow field is needed in order to determine which probes are best suited for these tests. In addition,

improvements in the hot-wire system to facilitate recording the data will be investigated. Presently, the rms voltages must be hand recorded from a needle indicator on the system voltmeter.

Shakedown Tests

Tests in the wind tunnel have been initiated to characterize the flow field in the test section without the test cylinder installed. Both static pressures on the wind tunnel floor and pitot pressure profiles have been obtained. In addition, core flow static and total pressures were measured near the north and south sidewalls at the test section entrance.

The static pressure distribution, expressed as pressure coefficients, for a tunnel dynamic pressure of two inches of water is contained in Fig. 19. The core flow conditions measured near the south sidewall at the test section entrance are the references used to calculate the pressure coefficients. The data indicate that the variation in the floor static pressure across the test section entrance was less than one percent of the tunnel dynamic pressure. The slight positive pressure gradient in the downstream direction due to the increasing boundary layer thickness is also apparent. Similar static pressure profiles were obtained at tunnel dynamic pressures of 1 and 1.5 inches of water.

A kielhead probe was manually traversed between the floor and ceiling of the test section at the tunnel centerline four inches downstream of the test section entrance. A pressure profile obtained for a tunnel dynamic pressure of two inches of water, expressed in terms of pressure coefficients, is shown in Fig. 20. The profile shows a significant asymmetry between the ceiling and floor boundary layers as well as a core flow pitot pressure deficit of approximately 3.5 percent

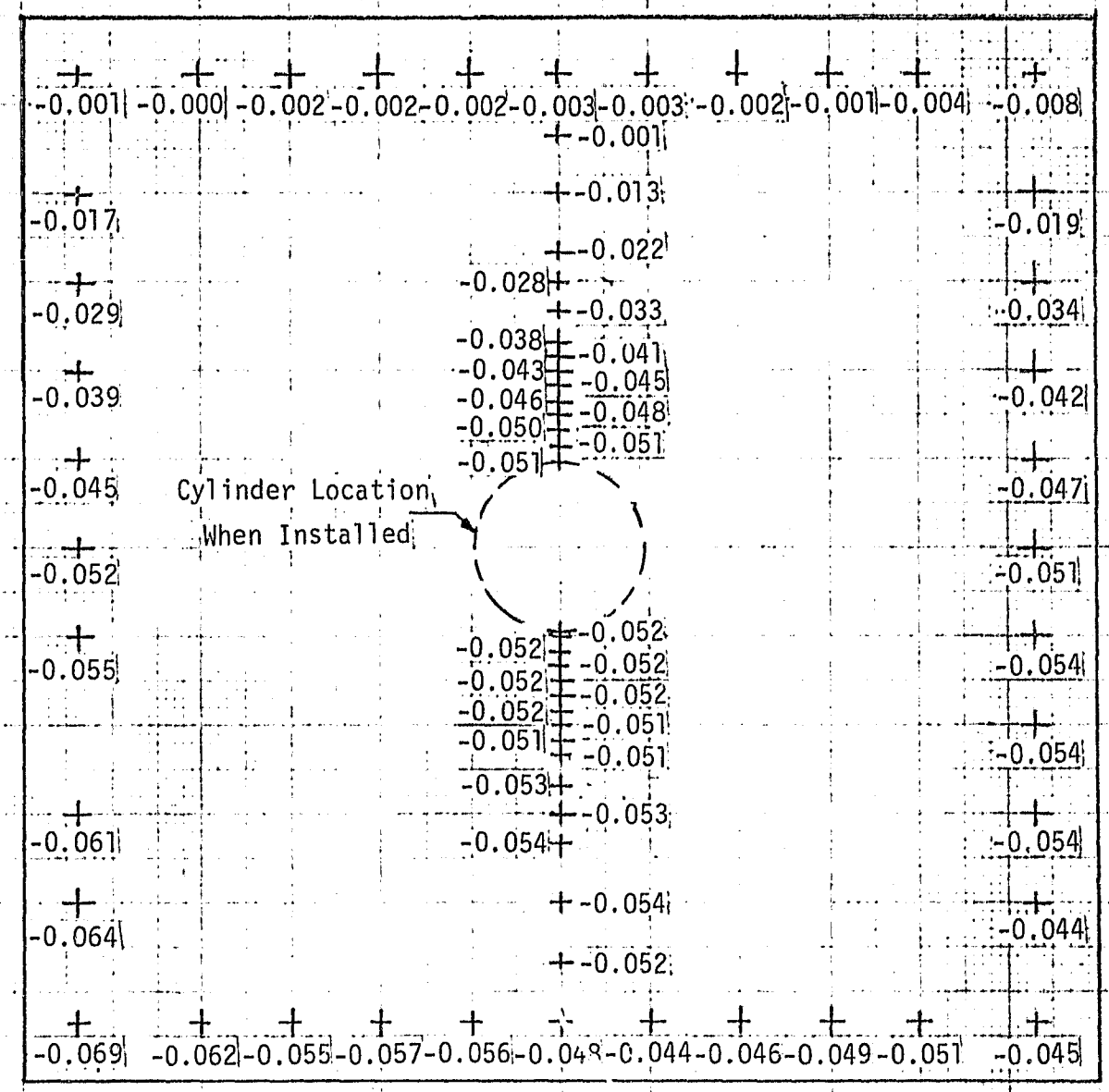

Figure 19. Static Pressure Coefficients on Test Section Floor

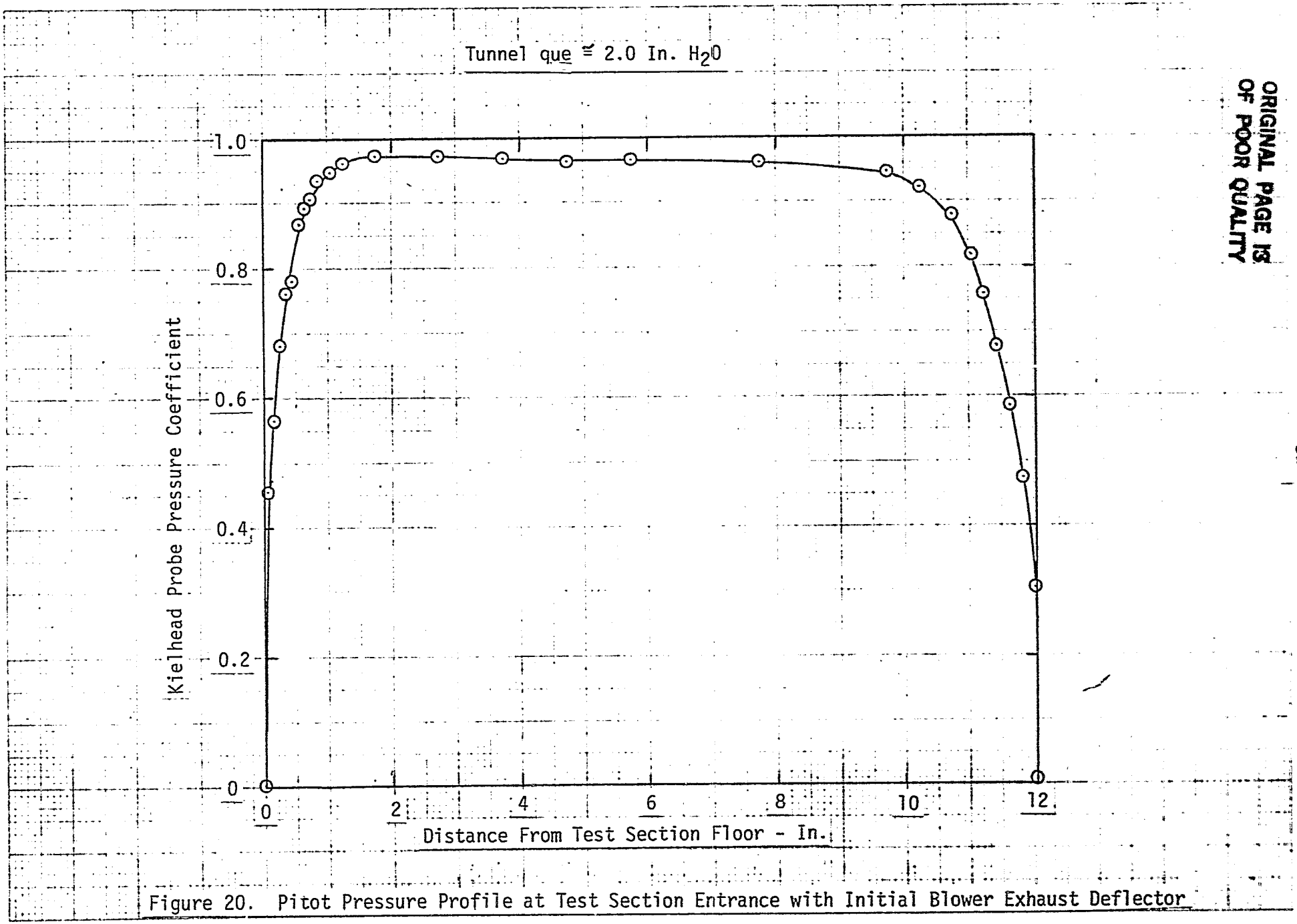

Figure 20. Pitot Pressure Profile at Test Section Entrance with Initial Blower Exhaust Deflector

relative to that measured near the south sidewall. Table I contains a summary of the calculated boundary layer parameters for the two boundary layers. A comparison of these parameters indicated the ceiling boundary layer thickness was more than twice that of the floor boundary layer. Also for these flow conditions, the pitot pressure measured near the north sidewall was approximately 2 percent less than that measured near the south sidewall. Thus, the core flow pitot pressure at the test section entrance was nonuniform along and asymmetric about the horizontal centerline.

A series of tests conducted to identify the cause of the nonuniformity in the flow at the test section entrance indicated that the exhaust flow from the tunnel blower was a major cause of the nonuniformity. The tunnel flow was exhausted vertically by the blower and turned forward toward the tunnel inlet by a shield. The momentum of the exhaust flow was large enough to set up a circulation around the tunnel as shown in Fig. 21. This circulation pattern evidently increased the flow entering the bottom of the inlet and reduced the flow entering the top of the inlet causing the differences measured in the upper and lower boundary layers. In addition, the recirculating flow was not uniform across the inlet. The blower exhausted the flow in a stream approximately three feet wide located over the south half of the tunnel. Thus, the recirculating flow could impose a lateral pressure gradient across the tunnel causing transverse nonuniformity in the core flow.

The recirculation pattern was significantly changed by installing another deflector on the tunnel plenum as shown in Fig. 22. The flow was deflected toward the north side of the laboratory allowing it to diffuse before reaching the inlet. This technique virtually eliminated the recirculation and the corresponding pitot pressure profile is shown in Fig. 23 along with the profile obtained without the

Table I
Boundary Layer Parameters For Initial Blower Exhaust Deflector

Tunnel Surface	δ in.	δ^* in.	θ in.	δ^*/θ
Floor	1.10	0.123	0.089	1.39
Ceiling	2.40	0.279	0.214	1.30

Table II
Boundary Layer Parameters With Modified Blower Exhaust Deflector

Tunnel Surface	δ in.	δ^* in.	θ in.	δ^*/θ
Floor	2.10	0.222	0.165	1.35
Ceiling	1.70	0.195	0.145	1.35

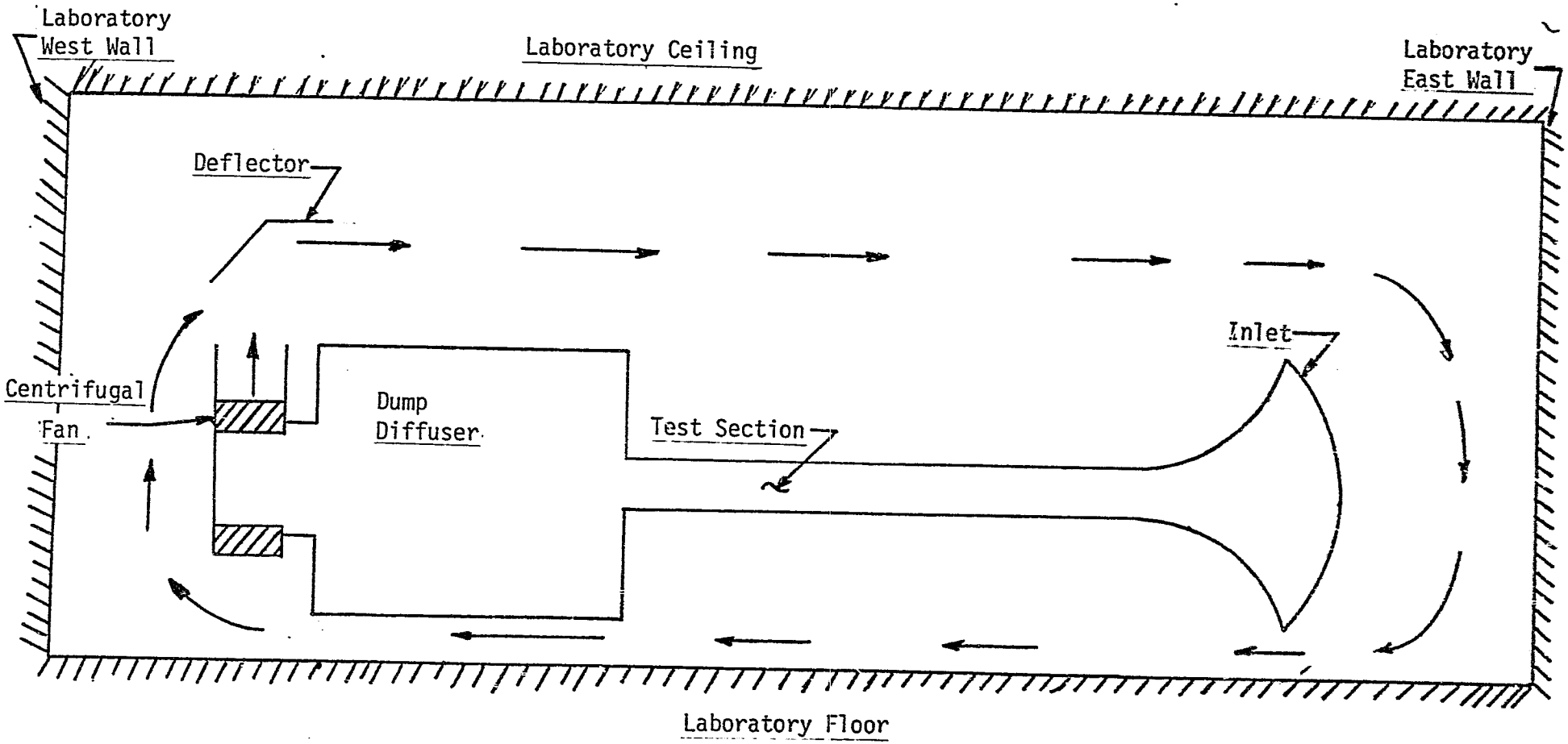

Figure 21. Side View of Recirculation Flow Pattern Around Wind Tunnel

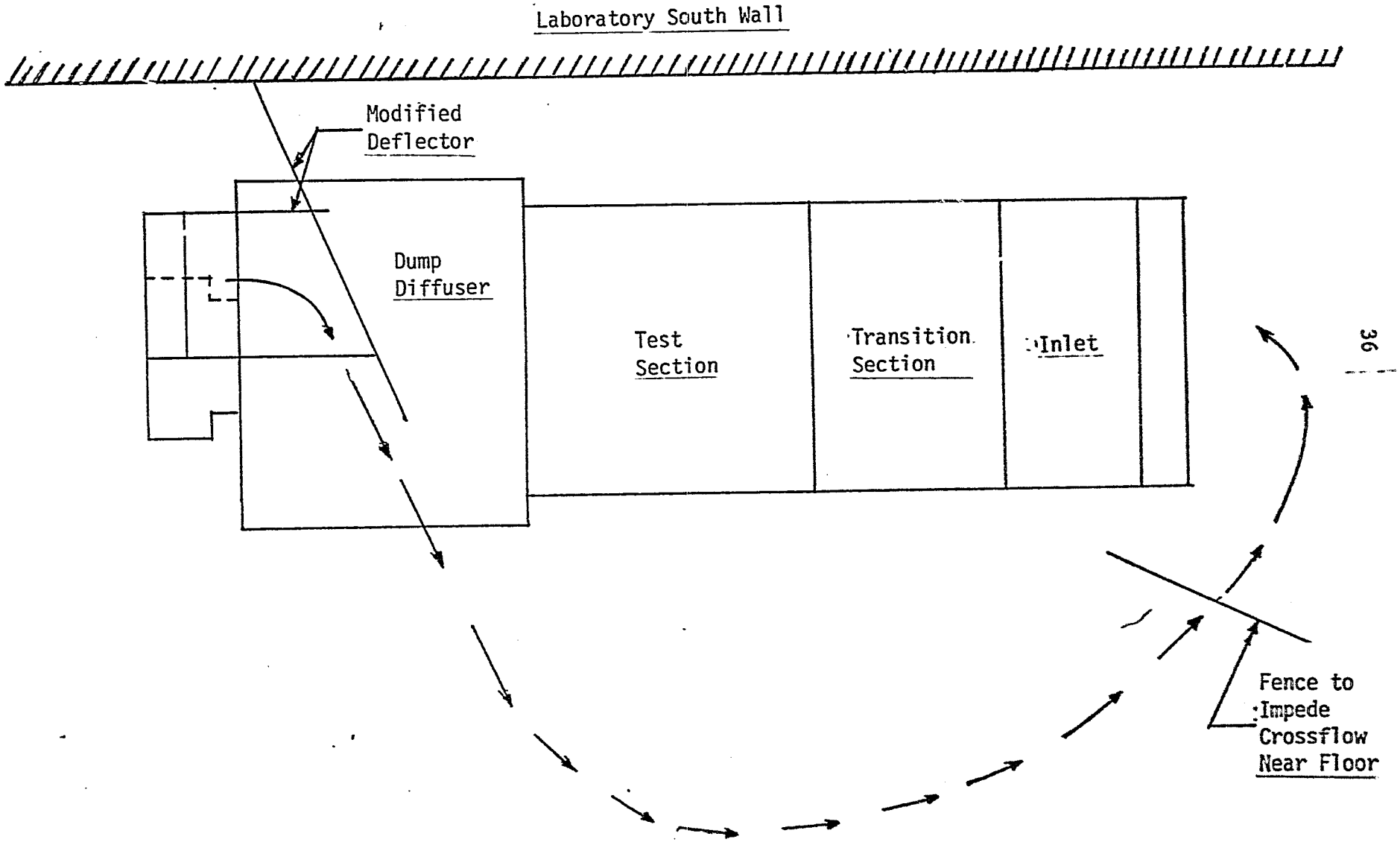

Figure 22. Top View of Wind Tunnel Showing Modified Deflector and Crossflow Fence

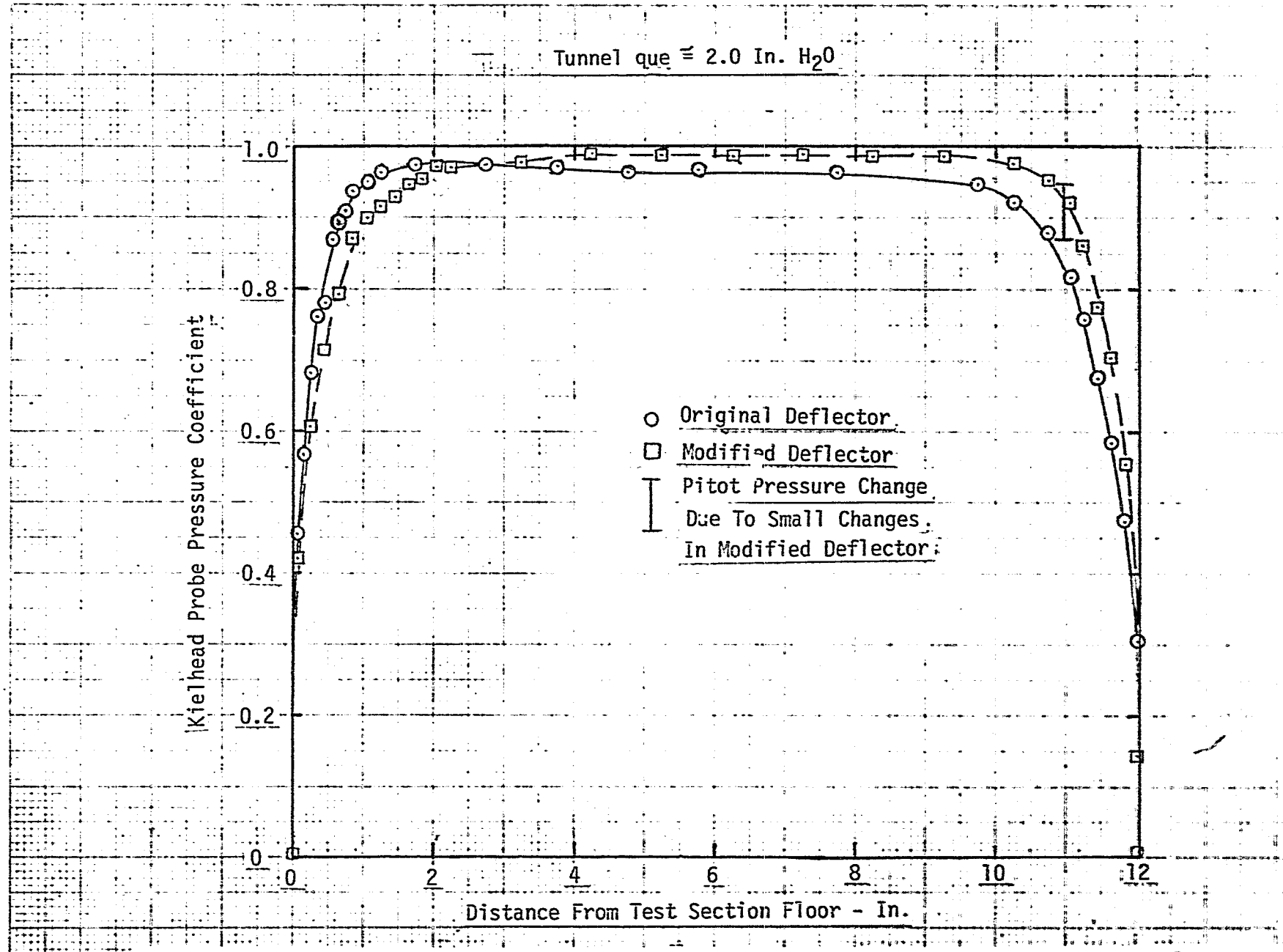

Figure 23. Pitot Pressure Profile at Test Section Entrance with Initial and Modified Blower Exhaust Deflector

deflector (Fig. 20). Deflecting the exhaust flow resulted in an increased floor and reduced ceiling boundary thickness. A comparison of the floor and ceiling boundary layer parameters, shown in Table II, shows that the boundary layers are more similar with the new deflector installed. The deflector also affected the transverse core flow pitot pressure distribution. The core flow pitot pressures measured near the north and south sidewalls were nearly identical while the centerline pressure was approximately 1 percent less than the sidewall pressures. Thus altering the exhaust flow pattern to eliminate the strong recirculation significantly improved the test section inlet conditions.

Although the flow conditions were significantly improved by the deflector, several problems must still be resolved. One problem with this new deflector configuration is indicated by the pitot pressure profile in Fig. 23. The defect in the pitot pressure profile approximately 2.5 in. from the test section floor was caused by a vortex that was formed on the laboratory floor and ingested into the tunnel inlet. This vortex is formed when an inlet flow is subjected to a crossflow as shown by De Siervi, et al.[7]. The vortex was eliminated by placing a fence next to the inlet (see Fig. 22) to stop the crossflow on the laboratory floor. A corresponding increase in pitot pressure was observed in the test section floor boundary layer. Thus, removal of vorticity induced into the inlet flow by the blower exhaust should further improve the flow uniformity. Another problem with this deflector configuration is that the tunnel flow is sensitive to small changes in the deflector configuration. For example, the band shown in Fig. 23 represents the range in pitot pressure measured at that location for small changes in the deflector configuration. Therefore, additional development is required to more effectively isolate the tunnel from the laboratory.

Two efforts are underway to address these problems. One effort involves installing a porous plate type barrier in front of the exhaust flow to more effectively diffuse the blower exhaust flow without establishing a dominant room flow as was created by the deflectors. The other area of development involves fabricating a settling chamber upstream of the tunnel inlet. A sketch of the proposed modification to the inlet is shown in Fig. 24. The settling chamber will include a mesh of honeycomb and screens to remove vorticity induced by crossflow in the laboratory as well as more effectively allign the flow with the inlet to provide more uniform flow conditions at the test section. The combination of these efforts should more effectively isolate the tunnel from room effects.

Asymmetric Model of Saddle Point Flow

As reported on in Ref. 6, the Oswatitsch model for singular points in a flow was extended to cover the case of an asymmetric saddle point. During this reporting period (July 1, 1982 - January 1, 1983), a new analytical derivation of this model was carried out. The new derivation now requires only five input parameters to be specified rather than the six required for the earlier derivation. Work continues on the final report on the asymmetric model, and a paper on the model is being written.

Acknowledgements

The work reported on here was carried out by Mr. Wayne A. Eckerle, a doctoral condidate in the Mechanical Engineering Department and by the principal investigator. Mr. William Sheridan and Mr. James Adams, both seniors in the

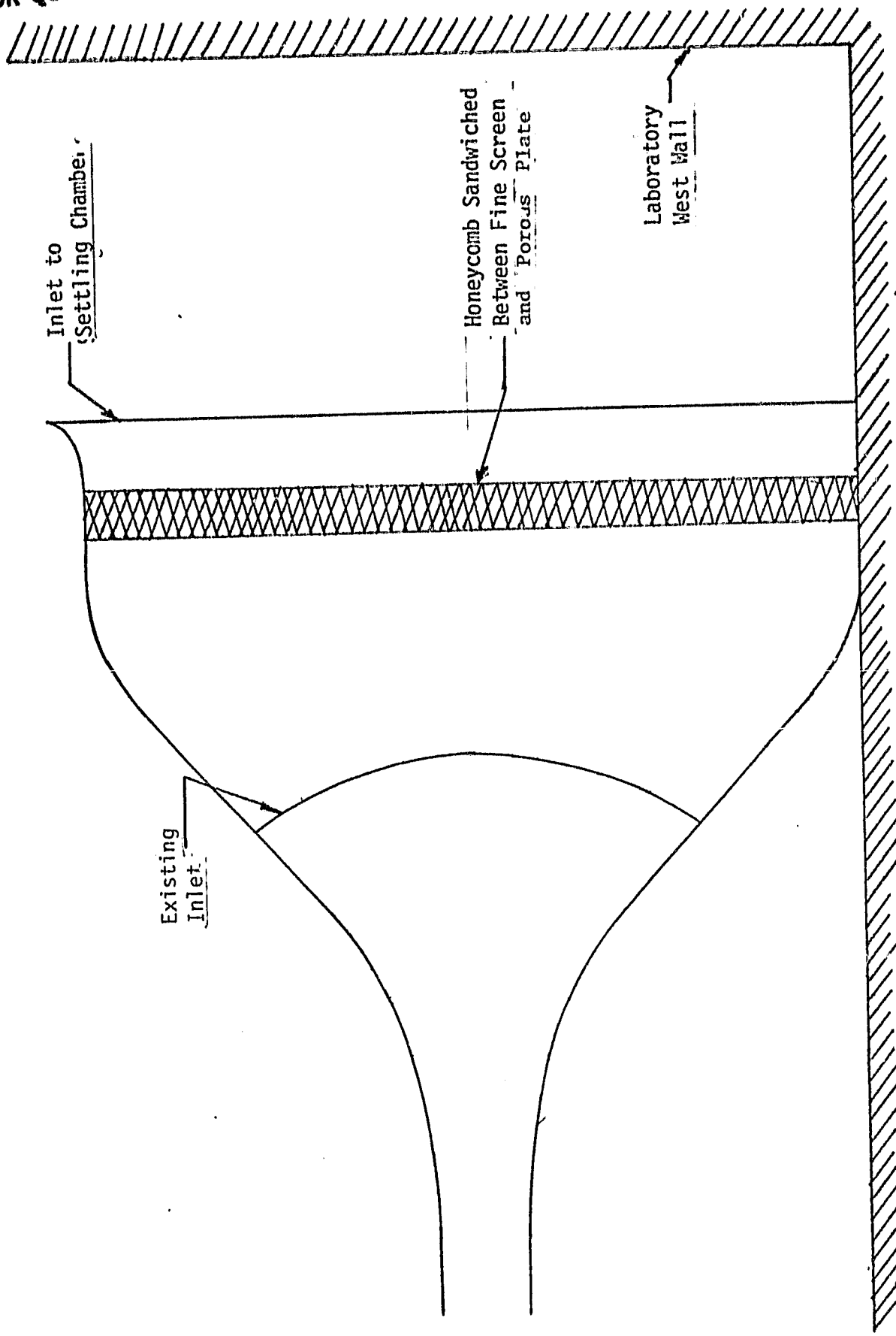

Figure 24. Proposed Settling Chamber for Wind Tunnel Inlet

Mechanical Engineering Department, worked on the probe positioner and the wind tunnel modifications.

References

1. Langston, L. S., "Turbine Endwall Two-Cylinder Program", Semi-annual Progress Report, January 1, 1979 - July 1, 1979.

2. Ibid., July 1, 1979 - January 1, 1980.

3. Ibid., January 1, 1980 - July 1, 1980.

4. Ibid., July 1, 1980 - January 1, 1981.

5. Ibid., January 1, 1981 - July 1, 1981.

6. Langston, L. S., "Turbine Endwall Single Cylinder Program", Semi-annual Progress Report, January 1, 1982 - July 1, 1982.

7. De Siervi, Viguier, H. C., Greitzer, E. M. and Tan, C. S., "Mechanisms of Inlet-Vortex Formation", Jour. of Fluid Mech., 124, pp.173-207, 1982.